NeuroImage 87 (2014) 490–504

Contents lists available at ScienceDirect

NeuroImage

journal homepage: www.elsevier.com/locate/ynimg

Analysis of task-evoked systemic interference in fNIRS measurements: Insights from fMRI

Sinem B. Erdoğan [a,*], Meryem A. Yücel [b], Ata Akın [c]

[a] Institute of Biomedical Engineering, Bogazici University, Kandilli, 34684 Istanbul, Turkey
[b] Athinoula A. Martinos Center for Biomedical Imaging, Department of Radiology, Massachusetts General Hospital, Harvard Medical School, Charlestown, MA, USA
[c] Department of Genetics and Bioengineering, Istanbul Bilgi University, 34060 Istanbul, Turkey

ARTICLE INFO

Article history:
Accepted 12 October 2013
Available online 19 October 2013

Keywords:
Hemodynamic response
Systemic interference
Functional near infrared spectroscopy
Magnetic resonance imaging
Physiological artifact removal
Cognitive task

ABSTRACT

Functional near infrared spectroscopy (fNIRS) is a promising method for monitoring cerebral hemodynamics with a wide range of clinical applications. fNIRS signals are contaminated with systemic physiological interferences from both the brain and superficial tissues, resulting in a poor estimation of the task related neuronal activation. In this study, we use the anatomical resolution of functional magnetic resonance imaging (fMRI) to extract scalp and brain vascular signals separately and construct an optically weighted spatial average of the fMRI blood oxygen level-dependent (BOLD) signal for characterizing the scalp signal contribution to fNIRS measurements. We introduce an extended superficial signal regression (ESSR) method for canceling physiology-based systemic interference where the effects of cerebral and superficial systemic interference are treated separately. We apply and validate our method on the optically weighted BOLD signals, which are obtained by projecting the fMRI image onto optical measurement space by use of the optical forward problem. The performance of ESSR method in removing physiological artifacts is compared to i) a global signal regression (GSR) method and ii) a superficial signal regression (SSR) method. The retrieved signals from each method are compared with the neural signals that represent the 'ground truth' brain activation cleaned from cerebral systemic fluctuations. We report significant improvements in the recovery of task induced neural activation with the ESSR method when compared to the other two methods as reflected in the Pearson R^2 coefficient and mean square error (MSE) metrics (two tailed paired t-tests, $p < 0.05$). The signal quality is enhanced most when ESSR method is applied with higher spatial localization, lower inter-trial variability, a clear canonical waveform and higher contrast-to-noise (CNR) improvement (60%). Our findings suggest that, during a cognitive task i) superficial scalp signal contribution to fNIRS signals varies significantly among different regions on the forehead and ii) using an average scalp measurement together with a local measure of superficial hemodynamics better accounts for the systemic interference inherent in the brain as well as superficial scalp tissue. We conclude that maximizing the overlap between the optical pathlength of superficial and deeper penetration measurements is of crucial importance for accurate recovery of the evoked hemodynamic response in fNIRS recordings.

Introduction

Functional near infrared spectroscopy (fNIRS) is a non-invasive imaging technique that utilizes near-infrared light for monitoring hemodynamic changes associated with evoked brain activity (Franceschini and Boas, 2004; Gibson et al., 2005; Obrig and Villringer, 2003). Over the past 15 years, fNIRS has become a complementary and alternative technique to functional magnetic resonance imaging (fMRI) with a high potential of use for clinical studies, cognitive, behavioral and neuroscience research (Boas and Dale, 2005; Lloyd-Fox et al., 2010; May et al., 2011). The advantages of fNIRS for studying brain activation include cost efficiency, possibility of use at the bedside, good temporal resolution, measurement of both oxy- (HbO) and deoxyhemoglobin (HbR) and use of non-ionizing radiation while the limitations include modest spatial resolution, lack of absolute quantification in continuous wave systems and limited penetration depth (Boas et al., 2004; Villringer and Chance, 1997).

A major concern with fNIRS measurements is the presence of strong spontaneous fluctuations or physiology-based systemic interferences in the signal due to cardiac pulsation (around 1 Hz), respiration (around 0.2 to 0.3 Hz) and a variety of spontaneous low frequency oscillations (LFOs) occurring in the range of 0.01–0.1 Hz (Obrig et al., 2000; Payne et al., 2009; Toronov et al., 2000). LFOs include the spontaneous oscillations in local vascular tone known as vasomotion (Gustafsson, 1993; Mayhew et al., 1996) and the systemic oscillations in arterial

* Corresponding author at: Institute of Biomedical Engineering, Bogazici University, Kandilli Kampusu, Cengelkoy, Istanbul, Turkey. Fax: +90 216 516 3479.
E-mail addresses: burcu.erdogan@boun.edu.tr, berdogan83@gmail.com (S.B. Erdoğan).

1053-8119/$ – see front matter © 2013 Elsevier Inc. All rights reserved.
http://dx.doi.org/10.1016/j.neuroimage.2013.10.024

blood pressure known as Mayer waves which typically occur at 0.1 Hz (Julien, 2006). Such systemic interferences are present in both the cerebral and superficial layers (i.e. scalp and skull) of the head and reduce the accuracy of fNIRS for detecting brain activation (Tian et al., 2011). The contribution of systemic interference to fNIRS signal is intensified due to the back reflection geometry of the measurements (i.e., light is both emitted and received at the scalp surface) which increases the sensitivity of fNIRS measurements to systemic oscillations occurring in the superficial scalp tissue. Besides, while blood flow within the brain is stabilized by partial autonomic neural control (Zhang et al., 2002), blood flow at the scalp tissue is not regulated by this buffer mechanism and is influenced by systemic physiological changes to a greater extent. The accurate identification and reliable elimination of the physiological noise embedded in the fNIRS signals can improve the signal-to-noise ratio, and/or can enable the same signal-to-noise ratio with a shorter stimulus period. This goal is significant, as with decreased acquisition time and increased signal quality; larger subject populations including young children and hospitalized patients can be monitored in a shorter time while the effects of fatigue and adaptation are minimized (Gregg et al., 2010; Saager et al., 2011).

Several methods have been proposed in the literature to reduce the systemic interference in fNIRS signals. Low pass filtering is the most common application, as it can effectively remove high frequency systemic oscillations such as heart beat (Franceschini et al., 2003; Jasdzewski et al., 2003). However, the frequency spectrum of physiology-based systemic interferences such as respiration, LFOs, and very low frequency oscillations (VLFOs) significantly overlap with the frequency spectrum of functional hemodynamic response to brain activation. Frequency-based removal of these interferences can therefore, distort the temporal characteristics of the recovered brain activity signal. Other methods for removing systemic interference include adaptive subtraction of a cardiac waveform (Gratton and Corballis, 1995), direct subtraction of a "nonactivated" fNIRS waveform (Franceschini et al., 2003), state space estimation (Diamond et al., 2006; Kolehmainen et al., 2003; Prince et al., 2003), wavelet filtering (Jang et al., 2009; Lina et al., 2008, 2010; Matteau-Pelletier et al., 2009) and principal components analysis (Franceschini et al., 2006; Zhang et al., 2005). There are also studies investigating the partial optical path lengths via Monte Carlo simulations of a layered human head model for multi-distance measurement set-ups (Umeyama and Yamada, 2009a,b; Yamada et al., 2009).

An extension to multi-distance measurement methods includes the use of additional short source-detector (SD) distance (usually less than 1 cm) channels together with typical long SD distance (about 3 cm) channels which are sensitive to both cerebral and extracerebral tissues. Short SD distance channel measurements probe superficial, extracerebral tissue only and are dominated by physiology-based systemic interference. To isolate and extract brain specific hemodynamic changes, these short SD distance channel measurements have been used to remove systemic interference from the long SD distance channel measurements with the assumption that a common systemic interference is present in both channel measurements (Gagnon et al., 2012; Gregg et al., 2010; Saager and Berger, 2005; Saager et al., 2011). Using multiple SD separations, an adaptive cancelation method has also been recently proposed and validated (Zhang et al., 2007a,b; Zhang et al., 2009). In contrast to the necessity of using short SD distance measurements, superficial hemodynamics can also be estimated by exploiting the photon time-of-flight distribution in time-domain NIRS at the expense of high-cost equipment (Aletti et al., 2012; Liebert et al., 2004).

Most of the above-mentioned methods are based on the assumption that systemic interference in fNIRS measurements is spatially homogeneous across the surface of the scalp. In the present study, we hypothesize that the spontaneous oscillations occurring in the brain tissue have a spatially global distribution, while the systemic interference coming from superficial scalp tissue has a more pronounced and localization-dependent effect on the fNIRS measurements. We treat both effects separately and propose an extended superficial signal regression method for canceling physiology-based systemic interference that is known to obscure the functional response to brain activation. To test our hypothesis, we apply our method on an optically weighted spatial average of the fMRI blood oxygen level-dependent (BOLD) signal which is obtained by combining weighted contributions from each voxel that coincide with the photon migration path. More specifically, for each subject and SD pair, once subject specific head models are obtained from structural MRI, photon-migration theory and Monte Carlo simulations are used to estimate the spatial sensitivity profile of light absorption changes that occur within different anatomical compartments of the head (as described in Boas et al., 2002). The overlap of this optical sensitivity profile with the voxels in each tissue layer (i.e. scalp, skull, CSF, gray matter and white matter) provides a means of predicting a spatially weighted BOLD response as a hemodynamic correlate of the fNIRS signal.

We evaluate the efficacy of removing systemic interference that occurs both in the brain and at the scalp tissue with our extended superficial signal regression (ESSR) method and compare its performance of physiological noise removal to i) a superficial signal regression (SSR) method where only superficial scalp interference is removed and ii) a global signal regression (GSR) method where it is assumed that systemic interference across all measurements is spatially global as proposed by most studies (Saager and Berger, 2005; Umeyama and Yamada, 2009b; Zhang et al., 2007a,b).

Although the data acquisition methods and signals in fNIRS and fMRI are different, it is well known that both methods are sensitive to the same hemodynamic changes. A number of studies involving concurrent fNIRS and fMRI recordings have shown that during functional brain activation, there is a strong correspondence between the local hemodynamic responses recorded by the two modalities (Huppert et al., 2006; Sassaroli et al., 2006; Steinbrink et al., 2006; Strangman et al., 2002; Toronov et al., 2001). Unlike fNIRS, fMRI has the advantage of probing brain tissue independent of the overlying scalp and skull layers. Signals from brain voxels are not mixed with superficial contamination but still are subject to cerebral systemic fluctuations interfering the brain functional response. To date, there have been no studies that have attempted to i) use scalp superficial interference measured by fMRI to construct a spatially weighted BOLD signal in which the true brain activity is embedded and ii) test the performance of various interference cancelation methods on such a hemodynamic correlate of the fNIRS signal.

Background

Photon migration theory

Near infrared imaging of the brain is based on measuring spatio-temporal variations in light absorption of the tissues between a source and a detector. Light is injected at the surface of the scalp, travels through extracerebral scattering tissues (i.e. scalp, skull and CSF) into the brain and again is received at the surface of the scalp. The photons emitted from the light source follow a statistical pattern and cross the scalp twice before being collected at the detector. In the wavelength range between 650 and 950 nm, the dominant absorbent chromophores are oxy- (HbO) and deoxyhemoglobin (HbR). Variations in the local concentrations of HbO and HbR (denoted as [HbO] and [HbR] respectively) modulate absorption properties of the brain in a wavelength dependent manner. The absorption coefficient at a given wavelength (λ) is linearly related to [HbO] and [HbR] through the equation:

$$\mu_a(\lambda) = \varepsilon_{\mathrm{HbO}}(\lambda)[\mathrm{HbO}] + \varepsilon_{\mathrm{HbR}}(\lambda)[\mathrm{HbR}] \quad (1)$$

where $\varepsilon_{\mathrm{HbO}}(\lambda)$ and $\varepsilon_{\mathrm{HbR}}(\lambda)$ denote the wavelength dependent extinction coefficients of each chromophore (Strangman et al., 2003). A change in these chromophore concentrations due to brain activation alters the

absorption coefficient and hence the detected light intensity. According to the modified Lambert–Beer law (MBLL), a small change in absorption coefficient is related to the change in measured optical density by the following formula:

$$\Delta \mathrm{OD}(t,\lambda) = -\log\left(\frac{\Phi(t,\lambda)}{\Phi_0(\lambda)}\right) = \Delta\mu_a(t,\lambda)L(\lambda) \quad (2)$$

where $\Phi(t,\lambda)$ is the average intensity of detected light, $\Phi_0(\lambda)$ is the average intensity of incident light and $L(\lambda)$ is the effective average pathlength of light through the tissue (Arridge et al., 1992; Boas et al., 2004; Cope and Delpy, 1988; Delpy et al., 1988). The effective pathlength is wavelength dependent but time-invariant when temporal absorption changes within the tissue are small. For a set of discrete volume elements (i.e., voxels) with each of them experiencing a different absorption change, the MBLL can be formulated as follows:

$$\Delta \mathrm{OD}(t,\lambda) = \sum_{j=1}^{\mathrm{Nvox}} \Delta\mu_{a,j}(t,\lambda)L_{i,j}(\lambda) \quad (3)$$

where $L_{i,j}(\lambda)$ is the effective pathlength of light for the ith measurement in the jth voxel (Boas et al., 2004). The spatial sensitivity profile of the photons can be determined with knowledge of the complex distribution of absorption and scattering properties of the tissues by empirical methods such as Monte Carlo based modeling (Boas et al., 2002; Wang and Jacques, 1995; Wang et al., 1995). For each channel, Eq. (3) can be written in matrix form as

$$y(\lambda) = A(\lambda)\cdot\delta x(\lambda) \quad (4)$$

where y represents the time-series of optical signal changes with respect to baseline, $\delta x(\lambda)$ represents the changes in absorption coefficient for each voxel, and A is a three-point Green's function matrix which describes the linear transformation from absorption changes of the underlying media to the measured optical signal change at each channel. The A matrix can be referred to as the 'photon absorption sensitivity profile' describing the spatial distribution of light traveling from a particular source to a detector (Arridge, 1999), and usually has a 'banana-shape' profile (a cross section of sensitivity profile is shown in Fig. 2).

Subjects and study design

fMRI data were collected from 18 healthy subjects during a mental arithmetic task. 3 subjects were excluded due to excessive motion artifacts and the results for 15 healthy subjects will be shown here for analysis (ten males aging 28.4 ± 3 and five females aging 28 ± 3.2). The study was approved by the Ethics Committee of Bogazici University and written informed consents were obtained from all subjects after complete description of the study prior to the first session. During fMRI measurements, subjects were positioned supine and asked to refrain from excessive movements and stay motionless. Instructions about the protocol were given from a screen over the subject's head. Each session started with a 30 second rest followed by a stimulation block of 39 s during which subjects were asked to serially subtract a 2-digit number from a 3-digit number (e.g., 146–84) and this block was followed by a 60 s of rest. This cycle was repeated 4 times. The arithmetic operations were displayed centrally in white color against a black background on a screen over the subjects' head. To avoid head movements, subjects were instructed to perform all tasks mentally, without vocalization or any movement of body.

fMRI data acquisition

A Philips 1.5 T MR system (Philips Systems, Best, The Netherlands) was used to acquire T1 weighted images using a gradient echo planar imaging (EPI) sequence with repetition time (TR) = 3000 ms, echo time (TE) = 50 ms, flip angle = 90°, matrix size = 64 × 64, 30 axial slices and voxel size = 3.59 mm × 3.59 mm × 2 mm. Structural scans were also taken from each subject using a T1 weighted magnetization-prepared rapid acquisition gradient echo (MPRAGE) sequence (0.9 mm × 0.9 mm × 1.2 mm resolution) to perform segmentation and coregistration. A time series of 142 scans were collected for each subject.

fMRI data processing was performed as follows: preprocessing steps consisting of motion and slice timing correction and temporal filtering with linear trend removal were performed on functional scans using SPM8 software (http://www.fil.ion.ucl.ac.uk/spm/, Wellcome Department of Imaging Neuroscience, UCL). The anatomical image was segmented into 5 tissue layers (gray matter, white matter, CSF, skull and scalp) and the segmented layers were unified to form a new anatomical image onto which the functional image is coregistered (Fig. 3).

The fNIRS probe (ARGES Cerebro, Hemosoft Inc., Turkey), for which we run photon migration simulations, contains 4 dual wavelength LED light sources and 10 photo-detectors arranged in a rectangular geometry. The sources and detectors are equidistantly placed on the probe with a nearest source-detector separation of 2.5 cm. Only SD pairs with minimum distance were considered resulting in 16 channels. During fMRI measurements, we placed a sponge-like probe housing on each subject's forehead with all the LEDs and detectors removed and their positions replaced with vitamin E gel capsules to mark source and detector locations on the MRI images (See Fig. 1).

Monte Carlo simulations of light transport in extra-cerebral and brain tissue

The forward matrix A (Eq. (4)) is a linear operator that projects absorption changes occurring at each volume element, to the measured optical signal between each SD pair. In our study, the A matrix is derived for each subject and channel and is used to estimate the contribution of hemodynamic changes occurring at each voxel to the total signal change observed at each particular SD pair. This forward model was formerly used to translate the hemodynamic changes observed within the fMRI space to the hemodynamic changes observed in the optical measurement space in a study by Huppert et al. (2006).

We performed Monte Carlo simulations of light transport on subject-specific tissue segmented anatomical MR images with optical properties taken from Strangman et al. (2003). The absorption (μ_a) and scattering coefficients (μ_s) at 760 nm were taken as 0.0177/0.73 (scalp), 0.0125/0.93 (skull), 0.0021/0.01 (CSF), 0.0195/1.18 (GM), and 0.0195/1.18 mm (WM). Anisotropy factor (0.9) and refract index (1.4) were assumed to be the same in all segmented tissues. The simulations were run by the program named Monte Carlo eXtreme (Fang and Boas, 2009), provided to the public by the Photon Migration Imaging Laboratory at Massachusetts General Hospital (http://mcx.sourceforge.net/cgi-bin/index.cgi).

To characterize absorption and scattering processes on realistic head models, source and detector positions were determined by identifying the location of vitamin E fiducial markers that were placed on the emptied spots of the fNIRS probe prior to the MPRAGE scans. After registering the locations of sources and detectors, Monte Carlo simulations of light transport were applied to the segmented anatomical head models generated for each subject and SD pair as described in Boas et al. (2002). The optical properties of white matter were set to those of gray matter due to the fact that changes in white matter properties have a negligible effect on the results (Boas and Dale, 2005). For each source and detector position, the trajectories of 10^8 photons were simulated at 760-nm in order to predict the spatial distribution of light traveling from a source position to a detector position. The spatial sensitivity matrices were calculated only for the closest SD pairs. Fig. 2 illustrates the spatial sensitivity profile of photon migration from a light source to a detector on an anatomical MRI image. The forward equation (Eq. (4)) sums voxel-wise changes in fMRI-BOLD signal over the volume using

the weights of the sensitivity matrix A to predict the measurements between each source-detector pair.

fMRI projection

The absolute BOLD signal intensity changes measured from each voxel are multiplied by the corresponding element of the optical forward matrix (A) projected onto the functional space. This is established by registering the forward matrices obtained within the high resolution anatomical image space to the lower resolution functional image space. A mask with an intensity of 1 for voxels with an optical sensitivity greater than the threshold (taken as 60 dB signal loss of the maximum sensitivity) and zero elsewhere is formed for each SD pair. BOLD signals from voxels within the intersection of this mask and scalp tissue are scaled with the corresponding optical weight and their summation is denoted as optically weighted scalp BOLD signal under that SD pair. The same procedure with gray matter mask is followed to calculate the optically weighted brain BOLD signal. Although we report results using the Green's function at 760 nm, the results were nearly identical when optical properties at 690 and 830 nm were used.

Signal model

Most neuroimaging techniques employ a standard analysis of functional brain activity signals with the assumption of a linear addition of hemodynamic changes (for further discussion, see Friston, 2007). BOLD signal from each SD pair contains the desired brain signal obscured by physiological noise. We will refer to the spatially and optically weighted BOLD signal for each SD pair as 'Sum' signal and model it as:

$$Y_{SUM} = Y_{BRAIN} + Y_{SUPERFICIAL}.$$

We investigated the possibility that the brain signal can be further decomposed into two components: one related with task induced neural activation ('neural signal') and one reflecting the effects of global systemic physiology ('global signal') occurring in the brain. We modeled brain signal for each SD pair as $Y_{BRAIN} = Y_{NEURAL} + Y_{GLOBAL}$. Hence, the physiological noise embedded in the Sum signal can be defined as

$$Y_{NOISE} = Y_{SUPERFICIAL} + Y_{GLOBAL}.$$

Regressing the superficial and global components from the Sum signal for each SD pair should then, in principle, produce a more accurate measure of the task induced neural activation: $Y_{SUM} - Y_{NOISE} = Y_{NEURAL}$ (Gregg et al., 2010). As an example, the contribution of superficial noise regressor is removed by regression $Y_R = Y_{SUM} - \alpha Y_{SUPERFICIAL}$ where Y_R is the residual signal after noise removal and $\alpha \equiv (Y_{SUM} \cdot Y_{SUPERFICIAL}) / (Y_{SUPERFICIAL} \cdot Y_{SUPERFICIAL})$ is the scaling coefficient that minimizes the root mean square of Y_R (Saager and Berger, 2008).

For each SD pair, an optically and spatially weighted sum of BOLD absolute signal intensity changes taken from scalp voxels along the photon migration path is used to construct a measure of hemodynamic changes localized to the superficial tissue layers ($Y_{SUPERFICIAL}$) whereas an optically and spatially weighted sum of BOLD absolute signal intensity changes from brain voxels within the photon migration path is used to construct a measure of hemodynamic changes occurring in the brain (Y_{BRAIN}). We scale the optically weighted scalp BOLD signals with a proportionality constant of 4/5 taking into consideration the

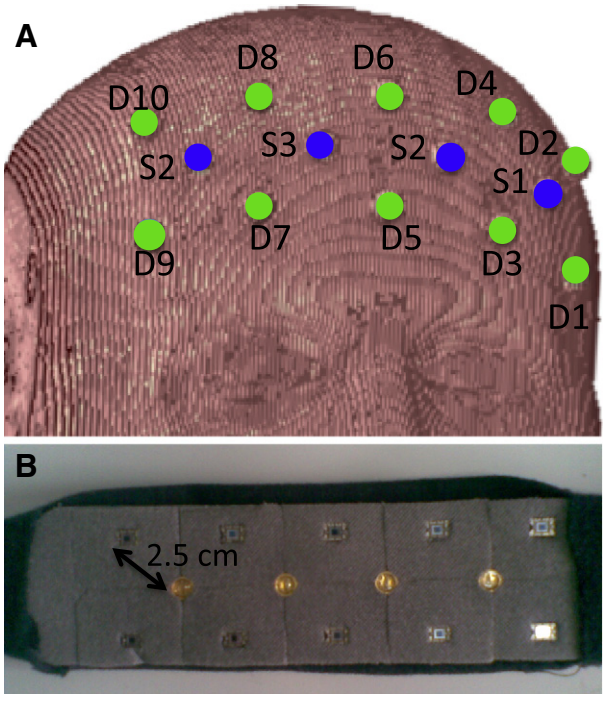

Fig. 1. (A) Location of fNIRS source and detectors on the constructed anatomical image. (B) Probe design. The fNIRS probe (ARGES Cerebro, Hemosoft Inc., Turkey) for which we run photon migration simulations contains 4 dual wavelength LED light sources and 10 photo-detectors arranged in a rectangular geometry. The source and detectors are equidistantly placed on the probe with an SD distance of 2.5 cm. During fMRI measurements, a sponge probe housing was placed on each subject's forehead with all the sources and detectors removed and their positions replaced with vitamin E gel capsules to mark source and detector locations on the MRI images.

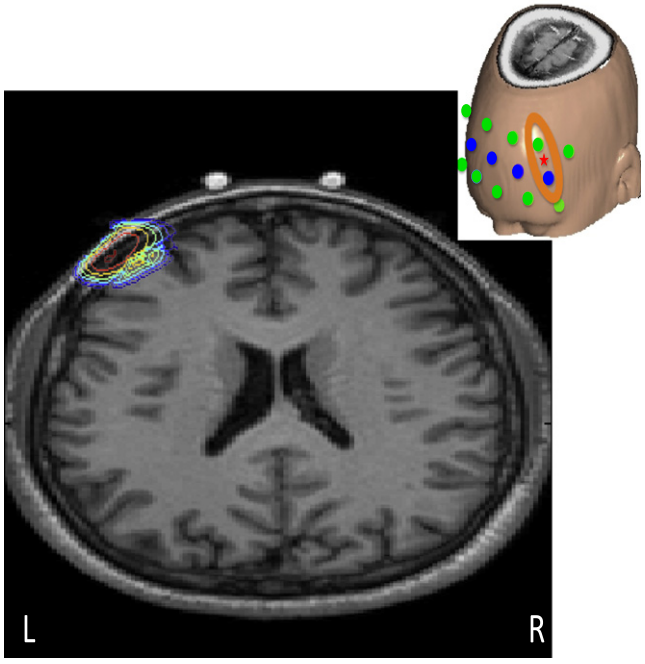

Fig. 2. Photon absorption sensitivity profile for an SD pair separated by 2.5 cm. For each subject, first a 3D realistic head model is generated, and then Monte Carlo simulations of light propagation are performed to obtain the spatial sensitivity profiles. The contour overlay is shown in logarithmic scale and contours are presented for each order of magnitude. The red star at the inset figure shows the location of this axial slice relative to the optical probe. The optically weighted Sum signal is obtained by multiplying BOLD activation at each voxel with the corresponding element of the sensitivity matrix A.

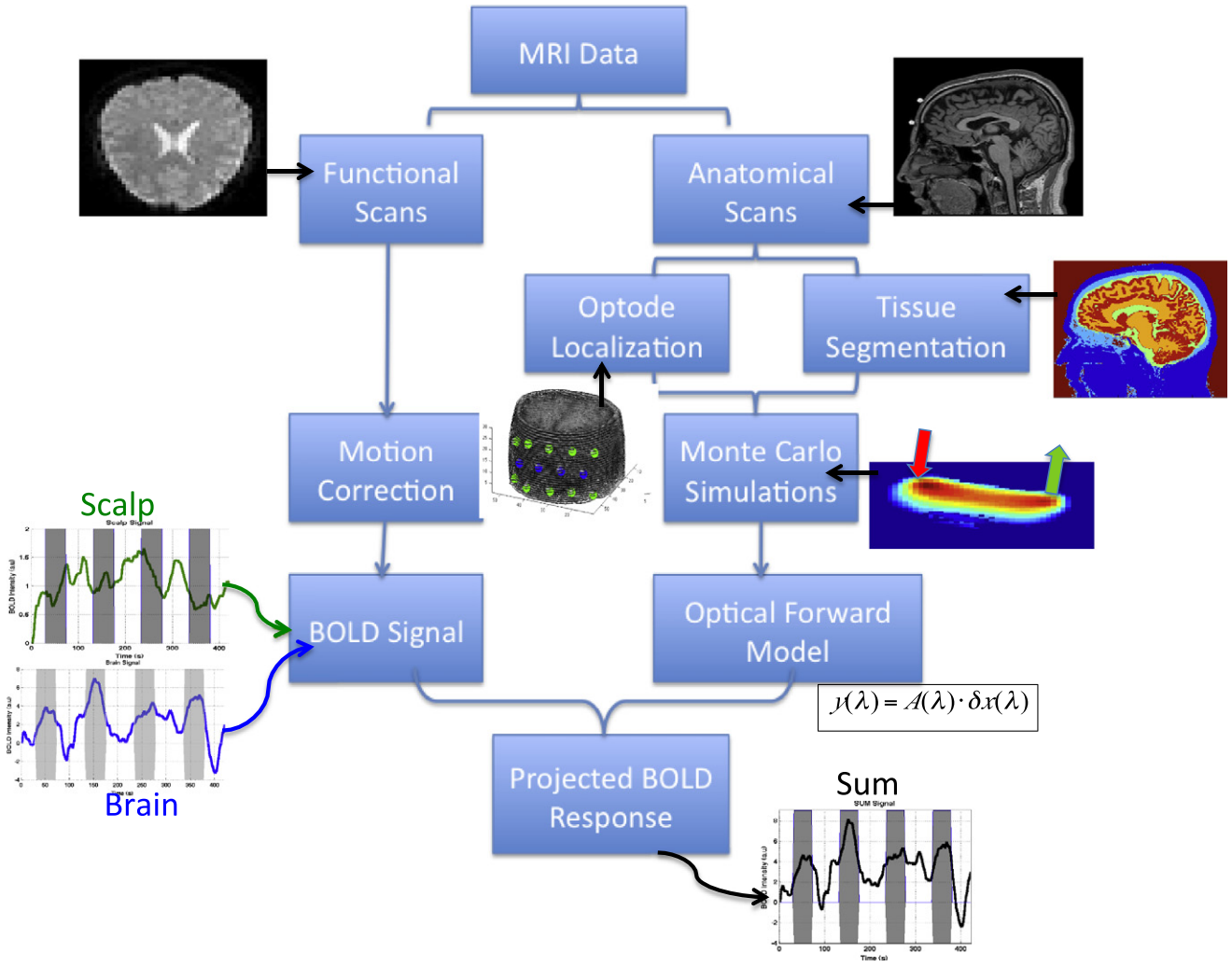

Fig. 3. Processing steps for functional and anatomical data. The anatomical images are coregistered and segmented into a five-layered model (skin, skull, CSF and gray and white matter). This image is used to perform Monte Carlo simulations to determine the light propagation through the head. The sensitivity weights obtained for each voxel are then used to scale each voxel's data and sum them for gray matter and scalp masks separately.

fact that i) BOLD signals obtained from the scalp mainly arise from intravascular signal changes, ii) they are affected in a more pronounced manner by the venous blood volume change rather than HbR concentration change and iii) at a magnetic field strength of 1.5 T with $T_E = 50$ ms and assuming a venous oxygen saturation of 70%, the change in venous blood volume with activation is estimated to contribute with a weight of ~4/5 to the total BOLD signal change observed in the scalp tissue (the details are discussed in Physics and physiology of brain and scalp fMRI signals and their relation to tissue absorbance measured with fNIRS section). Prior to formation of the Sum signals, motion parameters obtained from the preprocessing step are regressed out from all scalp and brain signals for a fair test of the three regression methods.

For each subject and SD pair, we simulated a 'short distance detector' placed close to the light source with a SD distance of approximately 1 cm. The position of each 'short distance detector' was arranged to maximize the overlap between the corresponding 2.5 cm distance SD measurement and the simulated short distance channel measurement. We then defined a region of interest (ROI) in the scalp tissue beneath the short distance detector and the source for each simulated short distance channel. The fMRI signals extracted from the voxels in each scalp ROI were averaged and denoted as 'superficial signals'. The average of all simulated superficial signals for each subject was denoted as 'global signal' and calculated as

$$G(t) = \frac{1}{N}\sum_{n-1}^{N} S_n(t) \tag{5}$$

where G(t) is a column vector representing the global signal change, $S_n(t)$ represents the superficial scalp signal change for the nth SD pair and N represents the total number of SD pairs for a subject ($N = 16$).

We attempt to quantify whether regressing the global or superficial signals alone is sufficient in retrieving the task induced neural signal. To explore the extent to which the Sum signal can be explained by the superficial signal, the Sum signals were regressed with the corresponding superficial signals for each subject. We call this method of eliminating superficial noise 'superficial signal regression' (SSR). In the second method, we regressed out the global signal from every Sum signal and called this method 'global signal regression' (GSR).

Last, we evaluate both SSR and GSR on Sum signals and name this method 'extended superficial signal regression' (ESSR). The residual time series v_i can be obtained by;

$$Y_{SUM}(t) = [G(t)S(t)]\beta + v_i(t) \tag{6}$$

where $Y_{SUM}(t)$ is the Sum data for a particular SD pair, $G(t)$ and $S(t)$ represent the global and superficial signals respectively, β is a vector of regression coefficients and v_i is the corresponding time series recovered after the global and superficial systemic signals are removed.

Data analysis

The performance of each regression method is determined by i) the Pearson correlation coefficient (R^2) and ii) the mean squared error (MSE) between task-related neural signal (neural) and the retrieved signal after each regression method. We also demonstrate the R^2 and MSE metrics between brain signal and the retrieved signals for comparison. The average of Pearson R^2 coefficients was calculated after applying the Fisher's r-to-z transformation and the resulting average is then back transformed (Devore, 1995). R^2 coefficient shows how well the two signals co-vary independent of scale. Because this metric is not an indicator of how well the amplitude of the retrieved signal matches that of the neural signal, we also interpreted the MSE metrics.

To compare the quality of the signals retrieved after each regression method, we evaluated the contrast-to-noise ratio (CNR) of the retrieved hemodynamic response. Contrast is defined as the peak-height of response (averaged over multiple stimulus presentations). We characterized measurement noise through the standard deviation in the pre-stimulus baseline. We judged each method's effectiveness by its improvement in CNR with respect to original Sum signal. CNR improvement is defined as

$$100 * \frac{(1 - CNR_A)}{CNR_B} \tag{7}$$

where CNR_B represents CNR for original Sum signal and CNR_A is the CNR of the signal after the listed regression method is applied.

In addition, the variation among four activation blocks is measured by calculating coefficients of variation (CV), denoted as $CV = \frac{\sigma}{\mu}$ where σ is the standard deviation across blocks and μ is the mean of each activation block.

We also investigated the effects of superficial noise and cerebral systemic physiology on the Sum signal by generating topographic maps of functional activation and analyzed their spatial patterns. The channel-wise hemodynamic responses during peak activation (taken as 14 s after stimulus onset) for each stimulus block are mapped onto forehead probe at the midpoint between each SD pair. The inverse distances calculated between each midpoint are used as weight factors to interpolate the peak responses over forehead. An image map is formed as shown in Fig. 5. We quantified the resemblance of each method's map to the neural activation map by calculating the mean square error between images as

$$\mathrm{MSE}_{\mathrm{method}} = \frac{1}{M} * \frac{1}{N} \sum_{i=1}^{M} \sum_{j=1}^{N} \left(I_{neural}^{i,j} - I_{method}^{i,j} \right)^2 \tag{8}$$

where N is the number of activation blocks (4 in this case), M represents the number of subjects, $I_{neural}^{i,j}$ represents the peak activation map obtained from neural signals for subject i, block j and $I_{method}^{i,j}$ represents the peak activation map obtained from listed method for subject i, block j.

Results

Fig. 4 presents time traces of the hemodynamic response to the mental arithmetic task from a single representative SD pair before and after optically weighting the scalp and brain signals (Figs. 4A and B respectively). The optically weighted Sum signal for each SD pair is assumed to be the fMRI correlate of the corresponding fNIRS signal while the optically weighted brain and scalp signals represent the stimulus related brain functional response and overlying superficial scalp physiological fluctuations respectively. Notice how the scalp signal is enhanced in terms of magnitude and how the brain signal is obscured by it in the Sum signal after weighing BOLD data from voxels along the photon migration path with the sensitivity matrix (Figs. 4C and D).

In Fig. 5, we examine the effect of applying GSR, SSR and ESSR on retrieving the time traces of the evoked brain hemodynamic response. A representative case of applying GSR, SSR and ESSR is shown in Fig. 5B. The original Sum signal fails to show a canonical response (Fig. 5A) due to superficial and cerebral systemic interferences. When only global signal is removed (GSR), it is difficult to distinguish individual activation epochs whereas application of SSR or ESSR results in a consistent canonical hemodynamic response. Task-evoked activations are apparent even before block averaging when either SSR or ESSR method is used (Fig. 5B); however ESSR results in higher response amplitudes. Applying SSR or ESSR decreases block-to-block variation while improving signal quality (Fig. 5C) whereas with GSR only, it is difficult to observe task-evoked activation even in the block-averaged data. Block averaged ESSR data has improved statistical significance with more time points showing a significant rise relative to baseline (Fig. 5C, asterisks mark sample points with a statistically significant deviation from prestimulus baseline of 5 s, $p < 0.05$ with a two-tailed t-test.). In this representative measurement, GSR did not yield a significant improvement in the CNR or quality of the hemodynamic response. SSR improved CNR by 60% whereas ESSR resulted in a CNR improvement of 240%. These traces (Figs. 5B–C) show the ability of ESSR to reduce noise and increase statistical significance.

The above-mentioned results can be generalized to the group data ($N = 240$) demonstrating a consistent increase in CNR and decrease in coefficient of variability (CV) as global and superficial signals are removed consecutively (Fig. 6A). The CNR values obtained using the ESSR method are significantly higher than those obtained using the GSR and SSR methods (two tailed paired t-test, $p < 0.05$). Moreover, the CNR values obtained for the original Sum signals are significantly lower than the CNR values obtained using the SSR and ESSR methods (two tailed paired t-test, $p < 0.05$). The CNR values obtained with the GSR method do not demonstrate a statistically significant difference from the CNR values obtained for the original Sum signals (two tailed paired t-test, $p < 0.05$). Similarly, CV values obtained using the ESSR method are significantly lower than those obtained with the GSR and SSR methods. Moreover, the CV values obtained for the original Sum signals are significantly higher than the CV values obtained using the ESSR method (two tailed paired t-test, $p < 0.05$). However no significance is observed between the CV values obtained using SSR and GSR methods.

Comparing %CNR improvement of the three methods shows that there are ameliorations in signal quality through the use of SSR or GSR alone, with SSR showing about 53% improvement while GSR results in an improvement of 24% among subjects showing positive improvement (Fig. 6B). There is a synergistic effect of utilizing both methods with the signal quality being highest after ESSR (60%). The %CNR improvements obtained for the original SSR and ESSR applied signals are significantly higher than the %CNR improvements obtained using the GSR method (two tailed paired t-test, $p < 0.05$).

Fig. 7 shows the summary of R^2 (A) and MSE (B) statistics over all subjects and measurements in a bar graph for each regression method. Correlation of scalp, brain and neural signals with corresponding Sum signals and the retrieved signals after each regression method is shown in Fig. 7A. Without any of the regression methods applied, scalp and Sum signals are highly correlated ($R^2 = 0.98$, $p < 0.05$) due to high sensitivity dominance of the scalp layer on the Sum signals. This finding is in accordance with a previous study by Takashi et al. (2011) who also showed a correlation of greater than 0.9 between near (5 mm) and far (30 mm) distance optical measurements which allowed them to probe skin, and a mixture of skin and brain measurements separately during a verbal fluency task. After the global signal is removed, mean correlation between Sum and scalp signals decreases to 0.68. This result indicates that the recovered signals after GSR still contain a common effect with

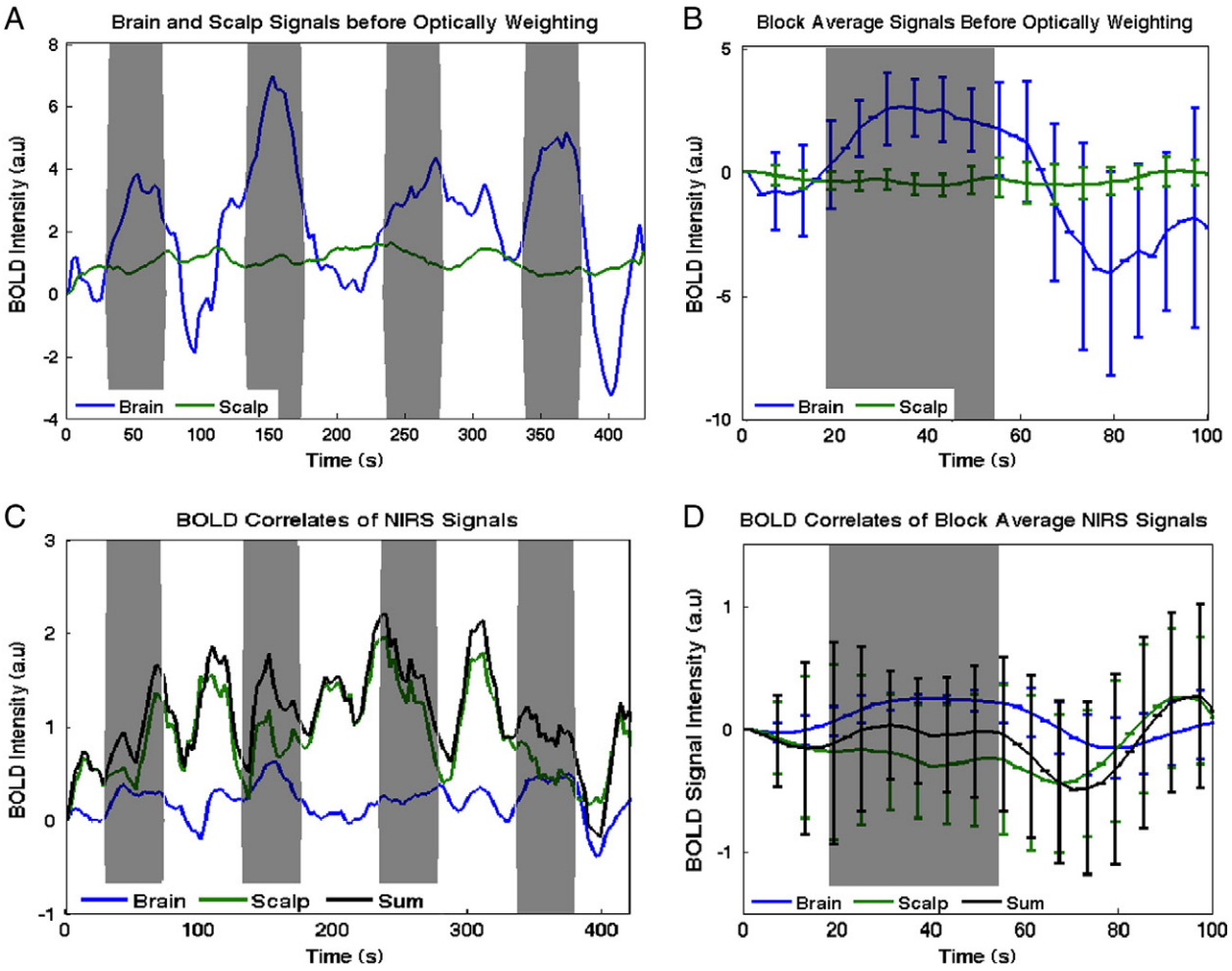

Fig. 4. Temporal traces of brain and scalp BOLD signals for a single SD pair (A) before and (C) after weighting with the optical sensitivity matrix. The scalp signal is highly correlated with the Sum signal ($R^2 = 0.92$) while the brain signal is weakly correlated ($R^2 = 0.35$). (B, D) Block averaged time traces of panels A and C respectively. Note how the brain BOLD signal is obscured in the Sum signal due to sensitivity preeminence of the scalp interference. Gray shaded regions indicate stimulus interval. The BOLD signal has arbitrary units.

the superficial scalp signals and suggests that GSR is not sufficient for removing the entire physiological noise in the Sum signal. However, correlation between scalp signal and Sum signal decreases dramatically after regressing out the superficial scalp signal (Fig. 7A), which shows that the superficial signal regression method successfully extracts the scalp interference from the Sum signal. For brain signals, the small but significant decrease in R^2 after global signal removal (0.29 to 0.25, $p < 0.05$) may be due to the fact that we have achieved to cancel the global effect in the Sum signals while it is still buried in the brain signals. SSR applied Sum signals are highly correlated with the brain signals ($R^2 = 0.98$, $p < 0.05$) whereas the correlation is slightly smaller when ESSR is applied ($R^2 = 0.96$, $p < 0.05$). The small but significantly higher R^2 with SSR applied Sum signals may be due to the fact when only the superficial noise is removed, the effect of cerebral systemic physiology is still preserved in the remaining Sum signal which contributes to the correlation with brain signal. Instead, when both global and superficial noises are removed from the Sum signal (ESSR method), the brain signals contain a systemic effect while the ESSR applied Sum signals do not. This causes SSR applied Sum signals to have a higher correlation with brain signals than the ESSR applied Sum signals ($R^2 = 0.98$ versus $R^2 = 0.96$ respectively, $p < 0.05$ two tailed paired t-test). As the correlation between neural and Sum signals is analyzed, an increasing trend in R^2 is observed with application of GSR and SSR. Correlation between the neural and Sum signals reaches a maximum when ESSR is applied ($R^2 = 0.99$, $p < 0.05$). This can be explained by the fact that when both superficial and global signals are removed from the Sum signal, the remaining signal better resembles the true task related neural activity, which is obtained by regressing out cerebral systemic effects from the brain signal.

The summary of MSE statistics over all subjects and measurements shown in Fig. 7B prove that a significant improvement in signal quality and resemblance to neural signal are obtained after ESSR. The same MSE statistics is also shown for the brain signals for comparison. There is a significant decrease in the MSE between the neural signal and the Sum signal when SSR is applied and the MSE is lowest when ESSR is performed.

Fig. 8 illustrates topographic images of a representative Sum signal (A), its scalp and brain components (B–C) as well as the Sum signal after GSR (D), SSR (E), ESSR (F) and the neural signal itself (G). Each column shows peak activation map from 4 consecutive stimulus blocks, for Sum (A), scalp (B), brain signals (C) and Sum signal after GSR (D), Sum signal after SSR (E) and Sum signal after ESSR (F). The last column (G) illustrates activation map for the neural signal. Block average and image variance of the 4 stimulus blocks are illustrated below the block images. The Sum image is greatly influenced by the fluctuations at the scalp and shows inconsistent localization of the hemodynamic responses from block to block. It is difficult to observe the localized brain activity in the Sum signal due to high dominance of the superficial scalp layer fluctuations (Fig. 8A, notice the variability among blocks 1–4) which tends to broaden some areas of activation while obscures some of them (compare second and third blocks of sum and brain images.) The brain map shows similar activations for each stimulus block, however the

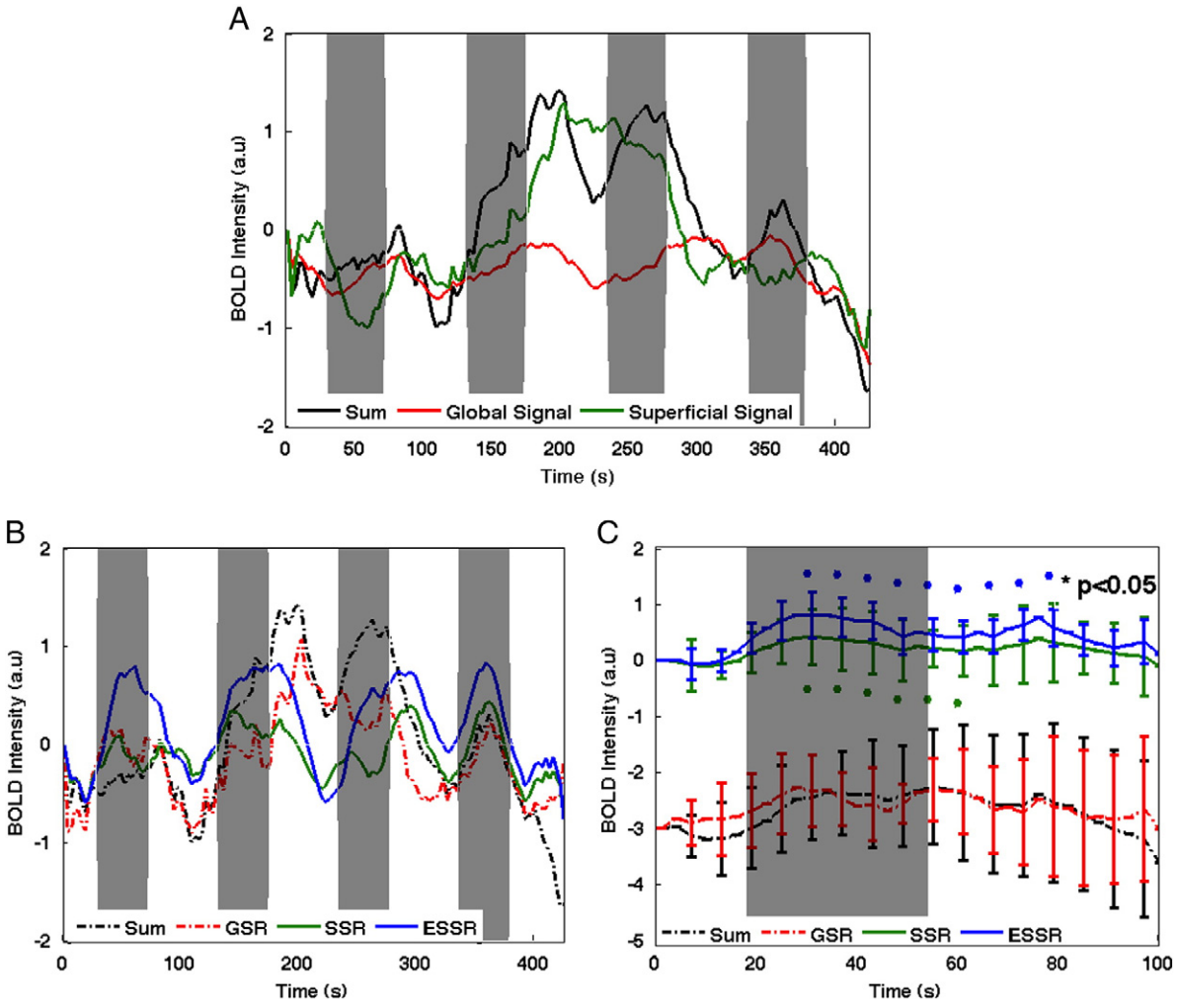

Fig. 5. Evaluation of the effect of GSR, SSR and ESSR on a representative Sum signal. Time traces of the Sum, global and superficial signals from 4 consecutive stimulus blocks (gray shaded regions) are illustrated in panel A. (B) Regressing out superficial noise signal from Sum signal produces SSR data whereas regressing out global noise signal produces GSR data. Regressing out both superficial and global signals produces ESSR data. (C) Block averaged time traces of panel B. The shape of activation becomes cleaner with SSR and ESSR while applying GSR only does not produce a pronounced effect (B, C). Error bars mark standard deviation and asterisks show statistically significant deviation from baseline (C). Variation among 4 blocks decreases while CNR is enhanced after applying ESSR. Note the reduced standard deviation and improved number of sample points showing statistically significant rise after ESSR method when compared to SSR and GSR methods.

neural map presents a more localized pattern of activation (compare blocks 1–4 of Figs. 8C and E). The ESSR images resemble the neural images most with the lowest mean square error. The mean square error (Eq. (8)) for Sum, GSR, SSR and ESSR images are 0.55, 0.43, 0.025 and 0.008 respectively.

Discussion

The major goal of our study is to compare the efficacy of removing physiological artifacts by performing i) a global signal regression (GSR), ii) a superficial signal regression (SSR) and iii) an extended superficial

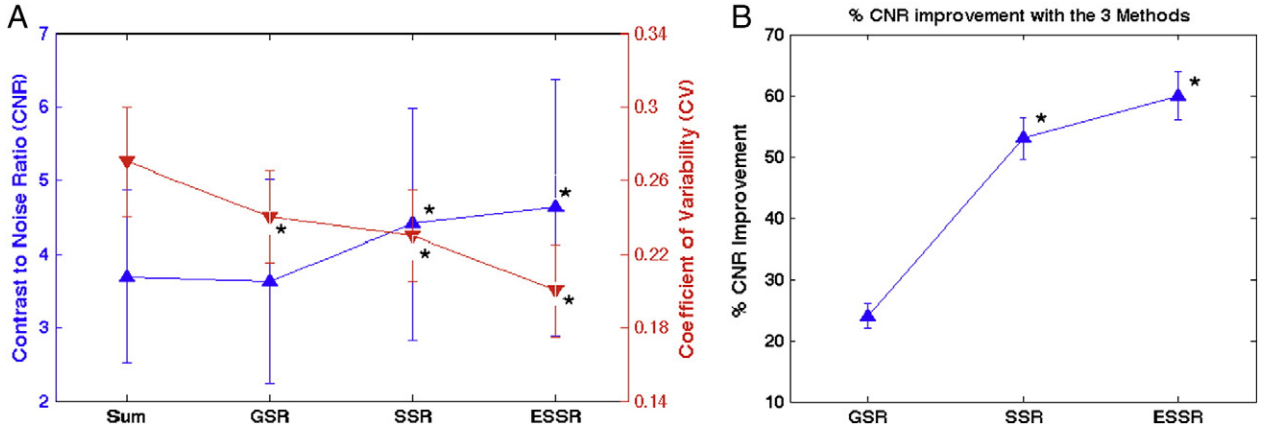

Fig. 6. (A) Grand average of the CNR and CV obtained for Sum data and after GSR, SSR and ESSR are applied. (B) %CNR improvement observed relative to Sum signal. The error bars show standard deviation across all measurements (N = 240). Statistically significant differences from the Sum Data are marked with an asterisk (2 tailed paired t-test, $p < 0.05$).

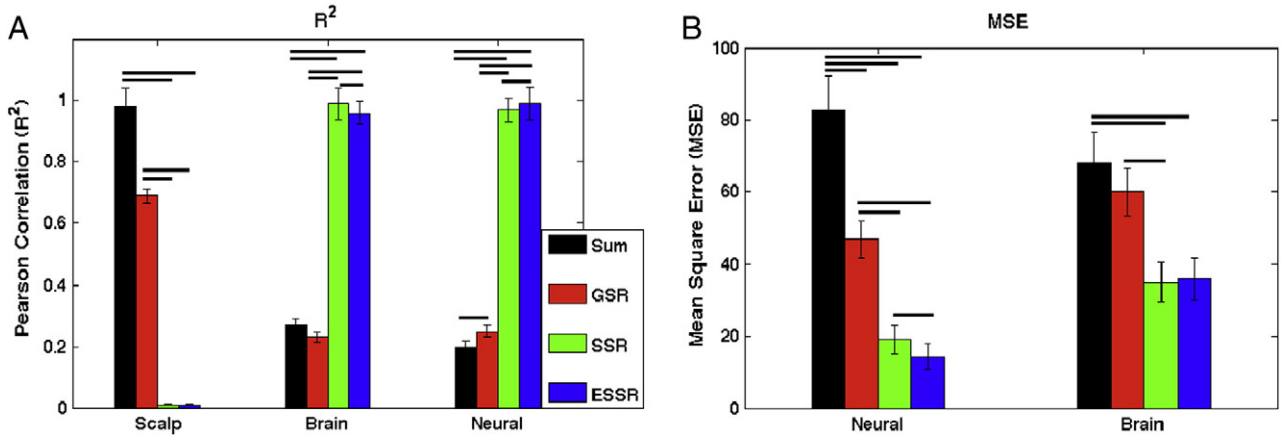

Fig. 7. (A) Correlation of scalp, brain and task induced neural activity related brain signal (neural) with Sum signal before performing any regression (Sum), after performing GSR, SSR and ESSR averaged for all subjects and measurements. Two tailed paired t-tests are performed between the R^2 computed for original Sum signals and the retrieved time series after each regression method. Statistical significance at $p < 0.05$ level are indicated by horizontal lines over the corresponding bars. (B) Mean Squared Errors (MSE) between the Sum signal and listed signals (neural and brain) before performing any regression on Sum signal, after performing GSR, SSR and ESSR. Two tailed paired t-tests are performed between the MSE computed for original Sum signal and the retrieved time series after each regression method. Statistical significance at $p < 0.05$ level are indicated by horizontal lines over the corresponding bars. The bars represent the means of 240 measurements and the error bars represent standard error of the mean.

signal regression (ESSR) where both a simulated superficial scalp measurement and a global signal are regressed out from each SD pair BOLD signal. A second, yet more physiologically relevant and innovative goal is to prove that ESSR produces signals with a higher resemblance to the true task related neural activity.

We determined the relative efficacy and performance of systemic interference removal methods with a spatially weighted BOLD signal. This procedure has some advantages over simulated data and data collected in fNIRS settings. For simulated data, there is a high chance that the quality of conclusions depends on the compatibility of the model being used. The performance of most algorithms have some uncertainty as the exploited mathematical methods work with assumptions made on signal dynamics or underlying physiological mechanisms (Sweeney et al., 2012). In an fNIRS setting, there is no access to an intact and uncorrupted brain signal because the brain signals are intermixed with the superficial physiological signals from the scalp. Unlike fNIRS, fMRI has the advantage of probing the brain tissue independent of the overlying scalp and skull layers. Signal from brain voxels is not mixed with superficial contamination but still is subject to cerebral systemic fluctuations interfering the brain's functional response. Superficial scalp BOLD signals collected from the overlap of the scalp mask with the photon sensitivity map contain physiological information from entire scalp tissue along the photon path. Hence, we investigated the effect of superficial contamination in a true setting in which we included physiological information from both where light is introduced and collected.

The fMRI-derived brain signals consist of a task induced neural activation intermixed with the effects of cerebral systemic fluctuations. We assumed that this neural activation signal is the “ground truth” for the desired task induced hemodynamic activity signal to be retrieved and quantify the performance and quality of each regression method by how well the retrieved signal resembles this ground truth neural signal. In the following, we will first briefly discuss the validity of our signal model and assess the improvements in signal quality and reproducibility of the results for the three methods. We will then provide some discussion about the physics and physiology of fMRI signals from the scalp and brain and the extent to which they can be used to quantify the fNIRS measurements obtained from both tissues.

Signal model

Two types of physiological fluctuations might interfere with the neuronal activation patterns embedded in fNIRS recordings: spontaneous oscillations that are not necessarily task correlated and that can be systemic and brain driven; and systemic changes such as blood pressure increases that are phase locked to the task-evoked experiment. The well-known systemic physiological interference is caused by cardiac beat around 1 Hz, respiratory oscillations around 0.4 Hz and low frequency oscillations (LFOs). The suppression of cardiac pulsations and respiratory oscillations is relatively easy because the correlation between the interference and the functional response of brain functional activity is usually low. LFOs in cerebral hemodynamics occur in the range of 0.01–0.1 Hz and arise from two main sources: spontaneous changes in local vascular tone referred to as vasomotion and the global oscillations in arterial blood pressure known as Mayer waves (Julien, 2006) affecting both the scalp and brain signals. In addition to spontaneous oscillations, some types of stimuli may cause a systemic response (i.e. an alteration in cardiac rate, blood pressure or respiration frequency) which can result in a change in baseline scalp or cerebral blood flow that correlates with the stimulus period. Such task-related systemic changes that are locked and dependent to the type of activation have been extensively investigated by previous studies (Kirilina et al., 2012; Minati et al., 2011; Scholkmann et al., 2013; Tachtsidis et al., 2009; Takahashi et al., 2011). One option for uncoupling these systemic changes and the task-induced neural activation is acquiring multi-distance fNIRS measurements assuming that the short distance measurements predominantly reflect scalp hemodynamics. The short distance measurement can then be removed from the long distance measurement, as performed in our simulations with the assumption that a similar superficial contribution is affecting both measurements (Gregg et al., 2010; Saager and Berger, 2008; Zeff et al., 2007). Superficial signal regression methods have been reported to attenuate both global physiological and task evoked extracerebral hemodynamic changes in optical data (Gregg et al., 2010; Zeff et al., 2007). In the ESSR method, we accounted for systemic and task-evoked interferences separately with a global and a local scalp regressor and achieved an enhanced signal quality with higher CNR and better resemblance to the neural activity related component of the Sum signal when compared to the other two regression methods. The ESSR method also successfully reduced the inter-trial variability in the Sum signal which most probably stems from the underlying spontaneous activity as suggested by Fox and Raiche (2007).

The physiological interference in fNIRS recordings can arise from the superficial scalp and skull tissue as well as the cerebral systemic oscillations in the brain tissue. Such physiological interference has been considered as a ‘global phenomenon’ previously (Gagnon et al., 2012;

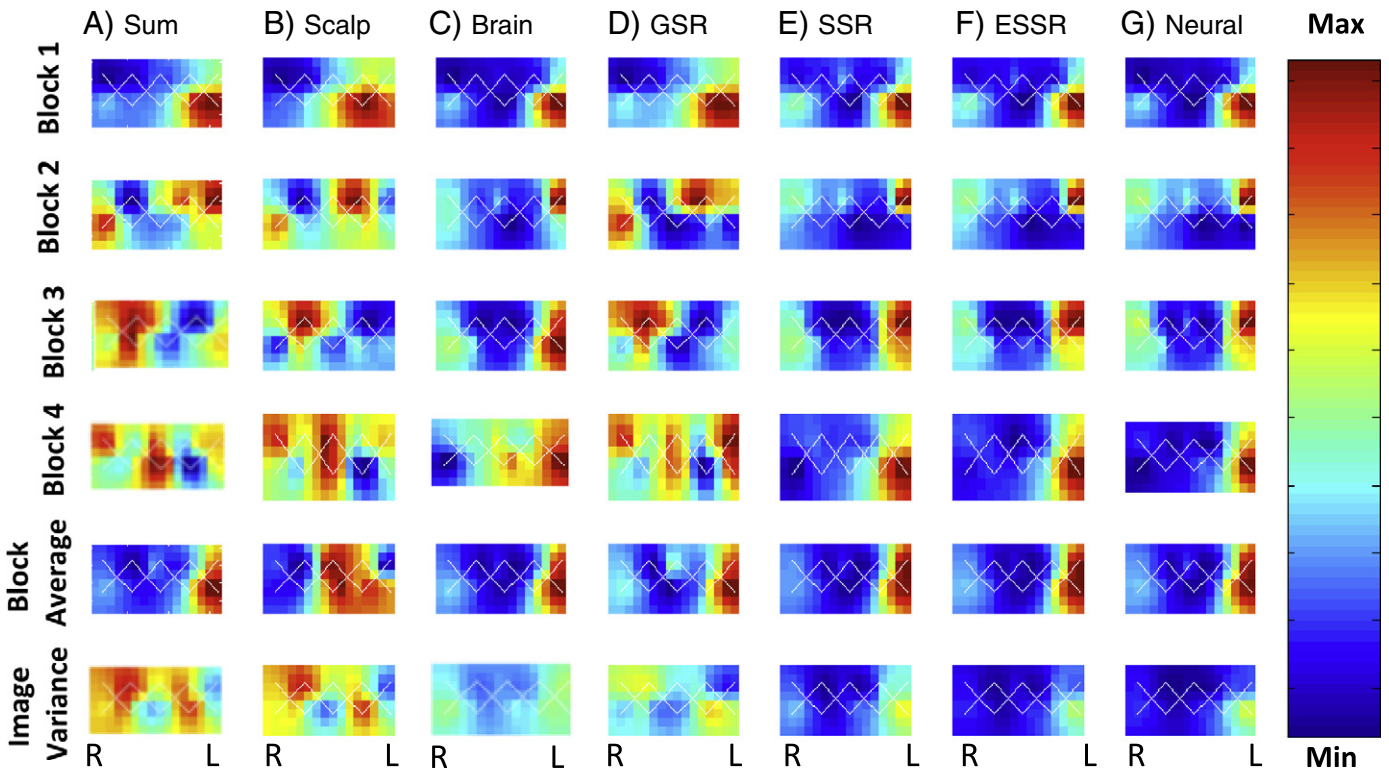

Fig. 8. (A) Evaluation of the effect of applying GSR, SSR and ESSR on image variance. Each column shows peak activation from 4 consecutive blocks for (A) Sum, (B) scalp, (C) brain signals and (D) Sum signals after GSR, (E) Sum data after GSR and (F) Sum data after ESSR. The last column (G) illustrates activation map for the neural signal. Block average and image variance of the 4 stimulus blocks are illustrated below block images. Note how the block activations look similar after performing ESSR. Image variance is displayed as the standard deviation of each SD pair at peak activation across all blocks. Image variance plot captures very little inconsistency in ESSR data.

Gregg et al., 2010; Saager and Berger, 2005; Saager et al., 2011; Umeyama and Yamada, 2009b; Zhang et al., 2007a,b). In contrast, we considered that the cerebral systemic oscillations have a global influence whereas the interference coming from superficial layers has a more pronounced localized effect on the fNIRS signals. Systemic oscillations affecting the brain are also present in the scalp tissue. Indeed, using long distance fNIRS measurements, Cooper et al. (2011) showed that low-frequency oscillations present in the fNIRS data correlated well with a large proportion of BOLD-fMRI voxels throughout the cortex. They suggested that the majority of low frequency contribution to the fNIRS signals occurs in the superficial layers of the head and future studies exploiting the use of superficial measurements, as regressors will be more convenient for eliminating low frequency noise in the BOLD data. Frederick et al. (2012) also showed that the short distance fNIRS signals provided better noise removal from the BOLD data when compared to long distance fNIRS signals. In accordance with these studies, we considered the simulated global and superficial scalp signals to be a good representation of the systemic interference common to both brain and scalp tissue as well as the more localized and dominant superficial physiological noise in the Sum signals.

The cerebral systemic interference present in our measurements is modeled by averaging the scalp signals from all the simulated short SD pair locations in the forehead. We assume the brain and scalp systemic variations to be correlated due to their close physiological and vascular connections as the heart, blood vessels, and lungs are the sources of the global pressure-induced oscillations, and the carotid artery is the common gateway for both scalp and brain hemodynamic oscillations (Zhang et al., 2007a). Also it is known that diploic and emissary veins can enable blood exchange between the extra- and intracranial compartments of the forehead through the skull (Zenker and Kubik, 1996). Therefore, we thought it is reasonable to take an average of all simulated scalp signals as a representative of global systemic physiology for each subject, which would attenuate variations common to all superficially sensitive channels and result in an enhanced waveform resembling the global interference in the brain. Similar approaches that used an average scalp regressor for removing global interference in the optical measurements were proposed previously in literature as well (Gregg et al., 2010; Mesquita et al., 2010).

Resemblance of the retrieved signals to the task related neural signal

Although the superficial scalp layer hemodynamic variations comprise a much larger portion of the total physiological interference due to sensitivity dominance of the scalp (Al-Rawi et al., 2001; Liebert et al., 2004), it is also necessary to account for the systemic physiological variations inherent in the brain when one attempts to retrieve the true neural activation in response to a task. A previous study by Huppert et al. (2006) noted the presence of a correlated temporal noise in concurrent fNIRS and cortical fMRI recordings and suggested that this noise did not originate from superficial scalp layer because their fMRI signals were obtained only from cortical tissues. Such physiological fluctuations have been noted in other fMRI and optical imaging studies as well (Bhattacharyya and Lowe, 2004; Toronov et al., 2000; Wise et al., 2004). We therefore modeled the effect of cerebral systemic interference in the brain signals with an average scalp regressor (details are discussed in the Signal model section) and examined the effect of applying GSR, SSR and ESSR on retrieving the time traces of the hemodynamic changes associated with this 'ground truth' signal resembling the desired neural activation (denoted as 'neural signal').

First, we tested whether regressing an average scalp regressor (similar to the work of Gregg et al., 2010) would successfully extract all of the systemic effect present in both layers and named this procedure a 'global signal regression' (GSR). From the changes in correlation between the scalp and Sum signal after GSR (Fig. 7A), we can conclude that GSR cannot filter all of the superficial contamination present in the Sum signal as the GSR applied Sum signals are still highly

correlated with scalp signals ($R^2 = 0.68$, $p < 0.05$). Moreover, the contrast to noise ratio is not enhanced significantly after GSR, and it is difficult to observe a canonical response in most of the measurements. Next, we tested the efficacy of removing the local superficial scalp signal from each measurement. We observed a substantial improvement in the signal quality as reflected in the CNR, R^2 and MSE metrics. When the superficial scalp signal is removed, the variation among blocks decreases (notice the decrease in CV in Fig. 6A and the error bars in Fig. 5C) to a better extent and it is easy to detect the canonical response at stimulus intervals for most of the measurements (an example is shown in Fig. 5B) even before block averaging.

By comparing the effects produced by GSR and SSR alone, we conclude that superficial scalp signal contribution to fNIRS signals varies significantly among different regions in the forehead and a local measurement is necessary for canceling the effects of superficial signal contamination adequately. A single global regressor did not contain the exact superficial noise information constrained to the overlying structures for each SD pair and was not able to recover the desired neural response accurately (note the MSE and R^2 statistics). This finding is in accordance with two recent studies which showed that the systemic interference in fNIRS measurements is not homogeneously distributed across the surface of the scalp (Gagnon et al., 2012) and the superficial task-evoked artifacts are more localized in the scalp draining veins (Kirilina et al., 2012). For the neural signals, a small increase in R^2 is accompanied by a small decrease in MSE with GSR applied Sum signals (Figs. 7A and B). Instead, there is a sharp increase in R^2 and a sharp decrease in MSE for SSR applied Sum signals. These results also demonstrate that superficial layer interference is the major component of the total systemic interference that is in accordance with the simulation and human subject findings by Zhang et al. (2007a,b).

In our study, we hypothesized that the cerebral systemic oscillations have a global effect whereas the superficial oscillations have a spatially heterogeneous effect. We accounted for both types of noise separately in the ESSR method and compared the retrieved signal with the neural signal that is considered to represent the 'ground truth' brain activation free from cerebral systemic oscillations. The correlation between neural and ESSR applied Sum signals is the highest while the MSE is the smallest when compared to the other two methods. The signal quality is enhanced most when ESSR method is applied with decreased variation among stimulus blocks, a clear canonical waveform, highest CNR improvement and a better resemblance to the ground truth neural activation signal. Application of ESSR method improves signal quality, reduces inter-trial variability by effectively canceling superficial scalp contamination as well as systemic interference inherent in the brain effectively. These improvements compared to GSR and SSR methods also suggest that our assumption of characterizing cerebral systemic physiology with the average of all scalp regressors is suitable for discarding the systemic components of the brain signal. The CNR and MSE metrics illustrate that we were able to recover the neural signal to a good extent. These results also show that ESSR method can reduce both spontaneous oscillations inherent in the brain and task-evoked extracranial effects during the mental arithmetic task.

Improvements in activity localization

We also investigated the effects of superficial noise and cerebral systemic physiology on the Sum signal by generating topographic maps of functional activation and their spatial patterns. We assessed the improvements in activation localization with the application of the above-mentioned regression methods. The Sum image is greatly influenced by the fluctuations at the scalp and shows inconsistent responses from block to block due to high dominance of the superficial scalp layer fluctuations (Fig. 5A, notice the variability among blocks 1–4). The effects of global and superficial systemic interference tend to blur the areas of activation (Fig. 8A). Such superficial scalp effects have been shown to worsen the signal-to-noise ratio, or be incorrectly interpreted as cerebral hemodynamic changes, resulting in false positives in fNIRS experiments previously as well (Kirilina et al., 2012; Minati et al., 2011; Tachtsidis et al., 2009; Takahashi et al., 2011).

The brain map shows similar activation patterns for each block. However, the neural map presents a more localized pattern of activation (compare blocks 1–4 of Figs. 8C and E). This improvement in localization of activity is most probably due to the cancelation of the global noise buried in the brain. Applying ESSR method reduces the effect of both the superficial scalp fluctuations and cerebral systemic physiology and gives rise to maps that very well resemble the neural maps. Although all activation maps appear similar after block-averaging (fifth row of Fig. 8), the greater noise in the Sum and scalp signals can be easily reflected in an image of variance map over multiple trials (sixth row of Fig. 8).

Comparison with other methods

In our study, we have implemented a computationally simple regression procedure for removing the effects of global and superficial interference during a cognitive task. Our work provides complementary information to previous fNIRS studies, which tested the efficacy of adaptive filtering and linear regression of scalp measurements during visual activation (Gregg et al., 2010; Saager et al., 2011; Zhang et al., 2009). Although adaptive filtering is a more powerful method than linear regression, Zhang et al. (2009) observed a mean improvement of 60% for 71% of their HbO_2 measurements and no CNR improvements were observed for HbR. Similarly, Saager et al. (2011) reported that 75% of the channels showed a CNR improvement while Gregg et al. (2010) observed an improvement of about 200% in CNR across all hemoglobin species in more than 80% of their subjects with linear regression. In our study, we observed a positive improvement in CNR for 62% of our measurements with a mean improvement of 60% with ESSR. The amplitude of the cerebral hemodynamic response in the prefrontal cortex during a cognitive stimulation may be smaller when compared to hemodynamic responses obtained from primary sensory or motor cortex during activation (Kirilina et al., 2012). For this reason, the CNR improvement obtained in our study may be smaller when compared to the CNR improvements observed during motor or visual stimulation in previous studies. Stimulus correlated systemic changes (e.g., increase in cardiac rate, arterial blood pressure, respiration frequency), can induce a false positive effect on CNR and regressing it out may result in an impairment of the CNR. Potential reasons behind the lower CNR improvement should be investigated in detail. Comparable performance of the ESSR method suggests that effective filtering can be obtained with simple, easily implemented algorithms.

The acceptance of fNIRS in clinical applications requires the delivery of reliable and robust signals from a greater percentage of subjects included in the studies. By canceling the effects of global and superficial systemic physiology, shorter studies with increased signal quality can be conducted on a greater number of subjects while the effects of fatigue and adaptation are minimized.

Physics and physiology of brain and scalp fMRI signals and their relation to tissue absorbance measured with fNIRS

Although our study relies on the similarity between fMRI and fNIRS signal changes observed during cognitive stimulation, there are several points to be considered when signals from the scalp and from the brain are compared for both modalities. fMRI signals from the brain have been shown to be sensitive to similar underlying hemodynamic changes with fNIRS signals (Toronov et al., 2000, 2003). However, regarding fMRI signals from the scalp, neither the biophysical origin nor how they can be related to scalp optical signals have been well-

investigated. In the following, we will discuss the physics and physiology of fMRI signals from the scalp and brain and how they can be related to temporal evolution of tissue oxygenation changes measured with fNIRS.

The most established theories of fMRI attribute the physiological origin of the BOLD signal to changes in local HbR content and blood volume (Boxerman et al., 1995; Buxton et al., 1998; Ogawa et al., 1993). The amplitude S of a single voxel MRI signal obtained with a gradient echo sequence with echo time T_E can be related to tissue water content M_v and relaxation time (T_2^*) as

$$S \sim M_v * \exp\left(-\frac{T_E}{T_2^*}\right). \quad (9)$$

There exist some fundamental differences when the theoretical frameworks used for interpreting brain and scalp fMRI signals are considered. The BOLD effect in the brain mainly arises from changes in local [HbR] which is reflected in venous blood relaxation time (T_2^*). In contrast, the scalp fMRI signals are thought to be primarily determined by venous blood volume M_v in a voxel. At 1.5 T field strength, while the extravascular contribution to the brain fMRI signals is responsible for half of the signal change (Buxton, 2002), the extravascular contribution to the scalp fMRI signals can be neglected due to low signal intensity. The tissue relaxation time (T_2^*) for skin is substantially shorter (~12 ms for the dermis) (Song et al., 1997; Weiss et al., 2001) than (T_2^*) of isolated blood (>80 ms) (Chien et al., 1994; Li et al., 1998; Silvennoinen et al., 2003). The intrinsically low scalp tissue signal is attributed to the short relaxation time of the skin layers (Richard et al., 1991; Song et al., 1997) and low effective proton density (Barral et al., 2010; Weiss et al., 2001) which can be regarded as a consequence of the fact that a significant portion of water molecules in the dermis is bound to collagen and not free (Richard et al., 1993). Therefore, task-related changes observed in the scalp fMRI signal reflect intravascular changes which may originate from a change in venous blood oxygenation and the related change in blood relaxation time T_2 or a change in venous water volume M_v or a combination of both (Kirilina et al., 2012). At a magnetic field strength of 1.5 T with $T_E = 50$ ms and assuming a venous oxygen saturation of 70%, the relative contribution of these biophysical mechanisms to the fractional BOLD signal change induced by activation can be estimated with the integrated model proposed by Uludag et al. (2009) as

$$\frac{\Delta S}{S} \approx 1.26 \frac{\Delta \sum \mathrm{HbO}}{\sum \mathrm{HbO} + \sum \mathrm{HbR}} + 0.4 \frac{\Delta \sum \mathrm{HbR}}{\sum \mathrm{HbO} + \sum \mathrm{HbR}} \quad (10)$$

where S is the venous MRI signal, $\sum$HbO and $\sum$HbR represent the baseline amounts of HbO and HbR, respectively, and ΔS, $\Delta\sum$HbO and $\Delta\sum$HbR represent the task-related changes of each quantity with respect to baseline. The reader is referred to Appendix 2 of Kirilina et al. (2012) and Uludag et al. (2009) for the derivation of Eqs. (9) and (10) and details of the underlying assumptions. Eq. (10) shows that for a single voxel scalp fMRI signal, changes in HbO content contribute with a weighting factor of 1.26, while changes in HbR content contribute with a weighting factor that is three times smaller. Kirilina et al. (2012) showed that, the scalp fMRI signals obtained during different cognitive tasks were highly correlated with scalp HbO concentration changes whereas they exhibited no significant correlation with HbR. Similarly, with simultaneous fNIRS and laser Doppler flowmetry recordings, Takahashi et al. (2011) demonstrated that blood flow and volume increased in the forehead scalp during performance of a verbal fluency task. However, no significant change in scalp HbR concentration was observed. The relative concentration changes of HbO and HbR measured by fNIRS correspond to the total change of $\Delta\sum$HbO and $\Delta\sum$HbR in the cutaneous veins which influence the fMRI signal according to Eq. (10). The fNIRS results obtained by the above-mentioned two former studies let us assume that for the scalp compartment $\Delta \approx \sum \mathrm{HbR} \approx 0$. Thus, the second term in Eq. (10) can be neglected and the venous volume change is reduced to $\frac{\Delta \sum \mathrm{HbO}}{\Delta \sum \mathrm{HbO} + \Delta \sum \mathrm{HbR}}$. To sum up, we infer that i) the scalp fMRI signal is directly proportional to venous volume change and ii) venous volume change is reflected in the scalp fMRI signal with a scaling factor of 1.26. For example, a 5% increase in scalp fMRI signal corresponds to a venous blood volume increase of about 4%.

Quantification of fNIRS signals with a spatially weighted fMRI signal

The fMRI-BOLD signal change originates primarily from the local concentration change of paramagnetic HbR molecules which results in an alteration of the magnetic susceptibility of blood and creates magnetic field inhomogeneities. Therefore, one would expect a correspondence between fNIRS-HbR and fMRI-BOLD signals. Numerous studies have been performed to explore correlations between fMRI and fNIRS signals both spatially and temporally (Huppert et al., 2005, 2006; Sassaroli et al., 2006; Strangman et al., 2002; Toronov et al., 2001, 2007). Although most theoretical approaches suggest a strong correlation between HbR and BOLD, experimental validation is a controversial issue. Some studies reported a better temporal correspondence between HbO and BOLD signals (Hoshi et al., 2001; Strangman et al., 2002), while other studies have shown a better correspondence between HbR and BOLD signals (MacIntosh et al., 2003; Siegel et al., 2003; Toronov et al., 2001). This discrepancy in literature may be related to the differential sensitivity of BOLD signal to vascular compartments in the presence of stronger or weaker static magnetic field (Boas et al., 2004; Cui et al., 2011). Nonetheless, a synthesis of the results from these studies indicates that, there is a strong correspondence between signals measured with fNIRS and fMRI.

By using the approach of BOLD signal projection through the optical sensitivity profile as performed in our study, the spatial and temporal correlation between the fNIRS and fMRI measurements could be examined with strong statistical temporal and spatial correlation in previous studies (Huppert et al., 2005; Sassaroli et al., 2006; Toronov et al., 2007). Huppert et al. (2005) indeed showed that the fNIRS-HbR and BOLD activation patterns are qualitatively consistent with one another after projecting the BOLD absolute image intensity signal from each voxel coinciding the photon migration path through the forward matrix that was found by the Monte Carlo simulations. Moreover, partial volume effects were avoided and the discrepancy in activation observed between fNIRS and fMRI recordings was corrected. Similarly, Sassaroli et al. (2006) found that a weighted average of the standard BOLD signal showed a strong spatial and temporal correlation with both HbO and HbR concentration changes measured with NIRS during a hand-tapping protocol. These studies support the spatiotemporal correspondence hypothesized to exist between the brain component of the spatially weighted Sum signal and the fNIRS signals.

Relative changes of the fMRI signal contain at least two contributions: one resulting from the tissue blood volume changes and the second resulting from tissue oxygenation changes. The fMRI signal changes due to the first mechanism are expected to be positively correlated with sum of concentration changes of HbO and HbR as measured with fNIRS. Taking into consideration i) the fact that task evoked superficial signal changes in the forehead during cognitive tasks were observed for HbO but not HbR (Kirilina et al., 2012; Takahashi et al., 2011), and ii) the striking similarity observed between the time courses of scalp fMRI and fNIRS HbO signals in a previous study (Kirilina et al., 2012), we suggest that fMRI signal changes observed in the scalp for our study may better represent the NIRS HbO or total hemoglobin (HbT) signal. Attributing the scalp fMRI signal changes to blood volume change is in accordance with the study of Drummond (1997) who reported an increase in forehead scalp blood flow during mental arithmetic, and suggested that the vasodilation is mediated by à-adrenoceptors. The scalp HbR content

is expected to be less affected by the task since task performance should not influence the metabolic demand of scalp. Consequently, we suggest that task-related hemodynamic changes in the forehead scalp during the mental arithmetic task may be due to the vasodilation mechanism. Some previous NIRS studies demonstrated significant changes in HbO signal from prefrontal cortex during mental arithmetic tasks. Hoshi and Tamura (1993) observed pronounced changes in HbO signal but not HbR during mental arithmetic in a 30-year-old male subject. Similarly, in the work of Tanida et al. (2004), mental arithmetic task caused increases in HbO and HbT concentration accompanied by a decrease in HbR in the right and left prefrontal cortices of all subjects. These results suggest that the brain component of the Sum signal might also better correlate with HbO or HbT changes measured with fNIRS. We therefore suggest that the spatially weighted Sum signal in our study may show better correspondence to the HbO or HbT signals measured with fNIRS.

Limitations of the study and recommendations for future work

One major limitation of our study is that we did not include any fNIRS measurements in the present work. Our analysis relies on a similarity between the time courses of fNIRS and fMRI signals instead of a quantitative comparison of the two modalities. Although the hemodynamic response measured with the two modalities might differ in terms of amplitude, the time course of the measured scalp hemodynamics has been shown to be very similar (Kirilina et al., 2012). A quantitative analysis of concurrent fMRI and fNIRS scalp measurements can help us elucidate the effect of task-related scalp hemodynamics on long distance NIRS measurements and will be our objective for future studies.

The systemic physiological parameters, especially the power of LFOs measured during an fMRI session might differ compared to the same parameters obtained in a sitting position during an fNIRS session (Heinzel et al., 2013; Tachtsidis et al., 2004). In the sitting position, the power of LFOs in both the scalp and brain tissue will be higher than that during the supine position. However, the majority of the low-frequency contribution to the fNIRS signal will still be from the superficial tissue as discussed in previous studies (Cooper et al., 2011; Tong and Frederick, 2010). Further studies on how posture affects the performance of the ESSR method in an fNIRS setting are necessary although we believe it is reasonable to assume that the superficial and global regressors obtained from the scalp measurements will still serve as a good modeling waveform for physiological noise during both postures.

One of the advantages of the ESSR method is its ease of use with any multi-distance fNIRS probe design, but this simplicity comes at the cost of making assumptions. One limitation is that there are likely several sources that contribute to the measured noise and that a multiple linear regression method combined with direct measurements of other systemic signals such as cardiac beat, breathing rate, and arterial blood pressure, may provide a better insight to understanding the effects of superficial and global interferences. Previous published work with 1.5 T field strength has shown that fMRI and NIRS are sensitive to similar underlying hemodynamic changes (Toronov et al., 2000, 2003). However, we should also note that fMRI signals obtained with 1.5 T MRI systems mainly reflect hemodynamic changes in venules and larger veins but not capillaries (Seiyema et al., 2004). fMRI data collected at higher magnetic field strengths ($\geq$4 T) will improve the sensitivity to capillaries and accuracy of proposed method.

The ESSR method is chosen for examination of task-evoked neural activity during a cognitive task; care should be taken in choosing the appropriate noise removal method for each experiment. As noted earlier, alternative methods for modeling the systemic physiology based interference in fNIRS recordings have been proposed in the literature. Each method is based upon different assumptions about the systemic noise present in fNIRS signals. While we tested only 3 methods for a single type of cognitive stimulation, a detailed study testing which interference cancelation method works best for which type of stimuli will be a valuable future contribution.

Conclusion

In this study, we have shown that treating superficial interference locally and cerebral interference globally with the ESSR method results in a more accurate recovery of the task-induced hemodynamic response with higher spatial localization and lower inter-trial variability when compared to the GSR and SSR methods. Using an average scalp regressor together with a local measure of superficial hemodynamics (ESSR method) better accounted for the systemic interference inherent in the brain. Our fMRI results demonstrate that i) superficial scalp interference is the major component of the total systemic interference and is not homogeneously distributed among different regions on the forehead, and ii) optical measurements of the brain hemodynamics are greatly influenced by interference of superficial origin. We conclude that maximizing the overlap between the optical path of the superficial measurements and the longer distance measurements is of crucial importance for accurate recovery of the evoked hemodynamic response in fNIRS recordings. A short optode (probing local scalp hemodynamics) placed close to each source and detector would be, in principle, ideal for accurate recovery of the evoked hemodynamic response in fNIRS recordings at the expense of impracticality. Future studies are needed to design optimal multi-distance probe geometries that account for superficial interference properly with the least number of short optode measurements.

Acknowledgments

This study is sponsored in part by BURF Project No.: 11XD4 and in part by TUBITAK Project No.: 112E034. Authors would like to thank Deniz Nevsehirli, Yasemin Keskin Ergen and Ali Bayram for their help in fMRI data collection, and the Photon Migration Imaging Laboratory at Massachusetts General Hospital for the Monte Carlo simulation code.

References

Aletti, F., Re, R., Pace, V., Contini, D., Molteni, E., Cerutti, S., Maria Bianchi, A., Torricelli, A., Spinelli, L., Cubeddu, R., Baselli, G., 2012. Deep and surface hemodynamic signal from functional time resolved transcranial near infrared spectroscopy compared to skin flowmotion. Comput. Biol. Med. 42, 282–289.

Al-Rawi, P.G., Smielewski, P., Kirkpatrick, P.J., 2001. Evaluation of a near-infrared spectrometer (NIRO 300) for the detection of intracranial oxygenation changes in the adult head. Stroke 32, 2492–2500.

Arridge, S.R., 1999. Optical tomography in medical imaging. Inverse Probl. 15, 14–93.

Arridge, S.R., Cope, M., Delpy, D.T., 1992. The theoretical basis for the determination of optical pathlengths in tissue: temporal and frequency analysis. Phys. Med. Biol. 37, 1531–1560.

Barral, J.K., Bangerter, N.K., Hu, B.S., Nishimura, D.G., 2010. In vivo high-resolution magnetic resonance skin imaging at 1.5 T and 3 T. Magn. Reson. Med. 63, 790–796.

Bhattacharyya, P.K., Lowe, M.J., 2004. Cardiac-induced physiologic noise in tissue is a direct observation of cardiac-induced fluctuations. Magn. Reson. Imaging 22 (1), 9–13.

Boas, D., Dale, A.M., 2005. Simulation study of magnetic resonance imaging-guided cortically constrained diffuse optical tomography of human brain function. Appl. Opt. 44 (10).

Boas, D.A., Culver, J.P., Stott, J.J., Dunn, A.K., 2002. Three dimensional Monte Carlo code for photon migration through complex heterogeneous media including the adult human head. Opt. Express 10, 159–170.

Boas, D., Dale, A.M., Franceschini, M.A., 2004. Diffuse optical imaging of brain activation: approaches to optimizing image sensitivity, resolution and accuracy. Neuroimage 23, S275–S288.

Boxerman, J.L., Bandettini, P.A., Kwong, K.K., Baker, J.R., Davis, T.L., Rosen, B.R., Weisskoff, R.M., 1995. The intravascular contribution to fMRI signal change: Monte Carlo modeling and diffusion-weighted studies in vivo. Magn. Reson. Med. 34, 4–10.

Buxton, R., 2002. Introduction to Functional Magnetic Resonance Imaging: Principles and Techniques. Cambridge University Press.

Buxton, R.B., Wong, E.C., Frank, L.R., 1998. Dynamics of blood flow and oxygenation changes during brain activation: the balloon model. Magn. Reson. Med. 39, 855–864.

Chien, D., Levin, D.L., Anderson, C.M., 1994. MR gradient echo imaging of intra-vascular blood oxygenation: T2* determination in the presence of flow. Magn. Reson. Med. 32, 540–545.

Cooper, R.J., Gagnon, L., Goldenholz, D., Boas, D.A., Greve, D.N., 2011. The utility of near-infrared spectroscopy in the regression of low-frequency physiological noise from functional magnetic resonance imaging data. NeuroImage 59, 3128–3138.
Cope, M., Delpy, D.T., 1988. System for long-term measurement of cerebral blood flow and tissue oxygenation on newborn infants by infrared transillumination. Med. Biol. Eng. Comput. 26, 289–294 (PubMed: 2855531).
Cui, X., Bray, S., Bryant, D.M., Glover, G.H., Reiss, A.L., 2011. A quantitative comparison of NIRS and fMRI across multiple cognitive tasks. NeuroImage 54, 2808–2821.
Delpy, D.T., Cope, M., van der Zee, P., Arridge, S., Wray, S., Wyatt, J., 1988. Estimation of optical pathlength through tissue from direct time of flight measurement. Phys. Med. Biol. 33, 1433–1442 (PubMed: 3237772).
Devore, J.L., 1995. Probability and statistics for engineering and the sciences. Simple Linear Regression and Correlation. Vol. 4th ed. Wadsworth Inc, Belmont, California, pp. 474–522.
Diamond, S.G., Huppert, T.J., Kolehmainen, V., Franceschini, M.A., Kaipio, J.P., Arridge, S.R., Boas, D.A., 2006. Dynamic physiological modeling for functional diffuse optical tomography. Neuroimage 30, 88–101.
Drummond, P.D., 1997. The effect of adrenergic blockade on blushing and facial blushing. Psychophysiology 34, 163–168.
Fang, Q., Boas, D.A., 2009. Monte Carlo simulation of photon migration in 3D turbid media accelerated by graphics processing units. Opt. Express 17, 20178–20190.
Fox, M.D., Raichle, M.E., 2007. Spontaneous fluctuations in brain activity observed with functional magnetic resonance imaging. Nat. Rev. Neurosci. 8, 700–711.
Franceschini, M.A., Boas, D.A., 2004. Noninvasive measurement of neuronal activity with near-infrared optical imaging. Neuroimage 21, 372–386.
Franceschini, M., Fantini, S., Thompson, J., Culver, J., Boas, D., 2003. Hemodynamic evoked response of the sensorimotor cortex measured noninvasively with near-infrared optical imaging. Psychophysiology 40 (4), 548–560.
Franceschini, M., Joseph, D.K., Huppert, T.J., Diamond, S.G., Boas, D., 2006. Diffuse optical imaging of the whole head. J. Biomed. Opt. 11 (5), 054007.
Frederick, B., Hocke, L.M., Tong, Y., 2012. Physiological denoising of BOLD fMRI data using Regressor Interpolation at Progressive Time Delays (RIPTiDe) processing of concurrent fMRI and near-infrared spectroscopy (NIRS). Neuroimage 60, 1913–1923.
Friston, K.J., 2007. Statistical Parametric Mapping: The Analysis of Functional Brain Images. Academic, London.
Gagnon, L., Cooper, R.J., Yücel, M.A., Perdue, K.L., Greve, D.N., Boas, D.A., 2012. Short separation channel location impacts the performance of short channel regression in NIRS. Neuroimage 59, 2518–2528.
Gibson, A.P., Hebden, J.C., Arridge, S.R., 2005. Recent advances in diffuse optical imaging. Phys. Med. Biol. 50, R1–R43.
Gratton, G., Corballis, P.M., 1995. Removing the heart from the brain: compensation for the pulse artifact in the photon migration signal. Psychophysiology 32, 292–299.
Gregg, N.M., White, B.R., Zeff, B.W., Berger, A.J., Culver, J.P., 2010. Brain specificity of diffuse optical imaging: improvements from superficial signal regression and tomography. Front. Neuroenergetics 2 (14), 1–8.
Gustafsson, H., 1993. Vasomotion and underlying mechanisms in small arteries. An in vitro study of rat blood vessels. Acta Physiol. Scand. (Suppl. 614), 1–44.
Heinzel, S., Haeussinger, F.B., Hahn, T., Ehlis, A.C., Plichta, M.M., Fallgatter, A.J., 2013. Variability of (functional) hemodynamics as measured with simultaneous fNIRS and fMRI during intertemporal choice. Neuroimage 71C, 125–134.
Hoshi, Y., Tamura, M., 1993. Detection of dynamic changes in cerebral oxygenation coupled to neuronal function during mental work in man. Neurosci. Lett. 150 (1), 5–8.
Hoshi, Y., Kobayashi, N., Tamura, M., 2001. Interpretation of near-infrared spectroscopy signals: a study with a newly developed perfused rat brain model. J. Appl. Physiol. 90, 1657–1662.
Huppert, T.J., Hoge, R.D., Franceschini, M.A., Boas, D.A., 2005. A spatial-temporal comparison of fMRI and NIRS hemodynamic responses to motor stimuli in adult humans. Optical Tomography and Spectroscopy of Tissue VI, Proc. SPIE 5693, p. 191. http://dx.doi.org/10.1117/12.612143 (May 05, 2005).
Huppert, T.J., Hoge, R.D., Diamond, S.G., Franceschini, M.A., Boas, D.A., 2006. A temporal comparison of BOLD, ASL, and NIRS hemodynamic responses to motor stimuli in adult humans. Neuroimage 29 (2), 368–382.
Jang, K.E., Tak, S., Jung, J., Jang, J., Jeong, Y., Ye, J.C., 2009. Wavelet minimum description length detrending for near-infrared spectroscopy. J. Biomed. Opt. 14 (3), 034004.
Jasdzewski, G., Strangman, G., Wagner, J., Kwong, K.K., Poldorack, R.A., Boas, D.A., 2003. Differences in the hemodynamic response to event-related motor and visual paradigms as measured by near-infrared spectroscopy. Neuroimage 20 (1), 479–488.
Julien, C., 2006. The enigma of Mayer waves: facts and models. Cardiovasc. Res. 70, 12–21.
Kirilina, E., Jelzow, A., Heine, A., Niessing, M., Wabnitz, H., Brühl, R., Ittermann, B., Jacobs, A.M., Tachtsidis, I., 2012. The physiological origin of task-evoked systemic artefacts in functional near infrared spectroscopy. Neuroimage 61 (1), 70–81.
Kolehmainen, V., Prince, S., Arridge, S.R., Kaipio, J.P., 2003. State-estimation approach to the nonstationary optical tomography problem. J. Opt. Soc. Am. A Opt. Image Sci. Vis. 20, 876–889 (PubMed: 12747435).
Li, D., Wang, Y., Waight, D.J., 1998. Blood oxygen saturation assessment in vivo using T_2^* estimation. Magn. Reson. Med. 39, 685–690.
Liebert, A., Wabnitz, H., Steinbrink, J., Obrig, H., Möller, M., Macdonald, R., Villringer, A., Rinneberg, H., 2004. Time-resolved multidistance near-infrared spectroscopy of the adult head: intracerebral and extracerebral absorption changes from moments of distribution of times of flight of photons. Appl. Opt. 43, 3037–3047.
Lina, J.-M., Dehaes, M., Matteau-Pelletier, C., Lesage, F., 2008. Complex wavelets applied to diffuse optical spectroscopy for brain activity detection. Opt. Express 16 (2), 1029–1050.
Lloyd-Fox, S., Blasi, A., Elwell, C.E., 2010. Illuminating the developing brain: the past, present and future of functional near infrared spectroscopy. Neurosci. Biobehav. Rev. 34, 269–284.
MacIntosh, B.J., Klassen, L.M., Menon, R.S., 2003. Transient hemodynamics during a breath hold challenge in a two part functional imaging study with simultaneous near-infrared spectroscopy in adult humans. NeuroImage 20, 1246–1252.
Matteau-Pelletier, C., Dehaes, M., Lesage, F., Lina, J.-M., 2009. 1/f noise in diffuse optical imaging and wavelet-based response estimation. IEEE Trans. Med. Imaging 28, 415–422.
May, L., Byers-Heinlein, K., Gervain, J., Werker, J.F., 2011. Language and the newborn brain: does prenatal language experience shape the neonate neural response to speech? Front. Lang. Sci. 2, 222. http://dx.doi.org/10.3389/fpsyg.2011.00222.
Mayhew, J.E.W., Askew, S., Zheng, Y., Porrill, J., Westby, G.W.M., Redgrave, P., Rector, D.M., Harper, R.M., 1996. Cerebral vasomotion: a 0.1-Hz oscillation in reflected light imaging of neural activity. Neuroimage 4, 183–193.
Mesquita, R.C., Franceschini, M.A., Boas, D.A., 2010. Resting state functional connectivity of the whole head with near-infrared spectroscopy Biomed. Opt. Express 1, 324–336.
Minati, L., Kress, I.U., Visani, E., Medford, N., Critchley, H.D., 2011. Intra- and extra-cranial effects of transient blood pressure changes on brain near-infrared spectroscopy (NIRS) measurements. J. Neurosci. Methods 197, 283–288.
Obrig, H., Villringer, A., 2003. Beyond the visible — imaging the human brain with light. J. Cereb. Blood Flow Metab. 23, 1–18.
Obrig, H., Neufang, M., Wenzel, R., Kohl, M., Steinbrink, J., Einhaupl, K., Villringer, A., 2000. Spontaneous low frequency oscillations of cerebral hemodynamics and metabolism in human adults. Neuroimage 12 (6), 623–639.
Ogawa, S., Menon, R.S., Tank, D.W., Kim, S.G., Merkle, H., Ellermann, J.M., Ugurbil, K., 1993. Functional brain mapping by blood oxygenation level-dependent contrast magnetic resonance imaging. A comparison of signal characteristics with a biophysical model. Biophys. J. 64, 803–812.
Payne, S., Selb, J., Boas, D.A., 2009. Effects of autoregulation and CO_2 reactivity on cerebral oxygen transport. Ann. Biomed. Eng. 37 (11), 2288–2298.
Prince, S., Kolehmainen, V., Kaipio, J.P., Franceschini, M.A., Boas, D., Arridge, S.R., 2003. Time-series estimation of biological factors in optical diffusion tomography. Phys. Med. Biol. 48, 1491–1504 (PubMed: 12817933).
Richard, S.B., Querleux, B.G., Bittoun, J., Idy-Peretti, I., Jolivet, O., Cermakova, E., Leveque, J.-L., 1991. In vivo proton relaxation times analysis of the skin layers by magnetic resonance imaging. J. Invest. Dermatol. 97, 120–125.
Richard, S.B., Querleux, B.G., Bittoun, J., Jolivet, O., Idy-Peretti, I., de Lacharriere, O., Leveque, J.-L., 1993. Characterization of the skin in vivo by high resolution magnetic resonance imaging: water behaviour and age-related effects. J. Invest. Dermatol. 100, 705–709.
Saager, R.B., Berger, A.J., 2005. Direct characterization and removal of interfering absorption trends in two-layer turbid media. J. Opt. Soc. Am. A 22, 1874–1882.
Saager, R.B., Berger, A.J., 2008. Measurement of layer-like hemodynamic trends in scalp and cortex: implications for physiological baseline suppression in functional near-infrared spectroscopy. J. Biomed. Opt. 13, 034017.
Saager, R.B., Telleri, N.L., Berger, A.J., 2011. Two-detector Corrected Near Infrared Spectroscopy (C-NIRS) detects hemodynamic activation responses more robustly than single-detector NIRS. Neuroimage 55, 1679–1685.
Sassaroli, A., de Blaise, F.B., Tong, Y., Renshaw, P.F., Fantini, S., 2006. Spatially weighted BOLD signal for comparison of functional magnetic resonance imaging and near-infrared imaging of the brain. Neuroimage 33 (2), 505–514 (PubMed: 16945553).
Scholkmann, F., Gerber, U., Wolf, M., Wolf, U., 2013. End-tidal CO_2: an important parameter for a correct interpretation in functional brain studies using speech tasks. Neuroimage 66, 71–79.
Seiyama, A., Seki, J., Tanabe, H.C., Sase, I., Takatsuki, A., Miyauchi, S., Eda, H., Hayashi, S., Imaruoka, T., Iwakura, T., Yanagida, T., 2004. Circulatory basis of fMRI signals: relationship between changes in the hemodynamic parameters and BOLD signal intensity. NeuroImage 21, 1204–1214.
Siegel, A.M., Culver, J.P., Mandeville, J.B., Boas, D.A., 2003. Temporal comparison of functional brain imaging with diffuse optical tomography and fMRI during rat forepaw stimulation. Phys. Med. Biol. 48, 1391–1403.
Silvennoinen, M.J., Clingman, C.S., Golay, X., Kauppinen, R.A., van Zijl, P.C.M., 2003. Comparison of the dependence of blood R_2 and R_2^* on oxygen saturation at 1.5 and 4.7 Tesla. Magnetic Resonance in Medicine 49, 47–60.
Song, H.K., Wehrli, F.W., Ma, J., 1997. In vivo MR microscopy of the human skin. Magn. Reson. Med. 37, 185–191.
Steinbrink, J., Villringer, A., Kempf, F., Haux, D., Boden, S., Obrig, H., 2006. Illuminating the BOLD signal: combined fMRI–fNIRS studies. Magn. Reson. Imaging 24, 495–505.
Strangman, G., Culver, J.P., Thompson, J.H., Boas, D.A., 2002. A quantitative comparison of simultaneous BOLD fMRI and NIRS recordings during functional brain activation. Neuroimage 17, 719–731.
Strangman, G., Franceschini, M.A., Boas, D.A., 2003. Factors affecting the accuracy of near-infrared spectroscopy concentration calculations for the focal changes in oxygenation parameters. Neuroimage 18 (4), 865–879 (PubMed: 12725763).
Sweeney, K., Ayaz, H., Ward, T., Izzetoglu, M., McLoone, S., Onaral, B., 2012. A methodology for validating artifact removal techniques for physiological signals. IEEE Trans. Inf. Technol. Biomed. 16 (5), 918–926.
Tachtsidis, I., Elwell, C.E., Leung, T.S., Lee, C.W., Smith, M., Delpy, D.T., 2004. Investigation of cerebral haemodynamics by near-infrared spectroscopy in young healthy volunteers reveals posture-dependent spontaneous oscillations. Physiol. Meas. 25, 437–445.
Tachtsidis, I., Leung, T.S., Chopra, A., Koh, P.H., Reid, C.B., Elwell, C.E., 2009. False positives in functional near infrared topography. In: Liss, P., Hansell, P., Bruley, D.F., Harrison,

D.K. (Eds.), Oxygen Transport to Tissue XXX. Advances in Experimental Medicine and Biology. Springer, US, pp. 307–314.
Takahashi, T., Takikawa, Y., Kawagoe, R., Shibuya, S., Iwano, T., Kitazawa, S., 2011. Influence of skin blood flow on near-infrared spectroscopy signals measured on the forehead during a verbal fluency task. Neuroimage 57, 991–1002.
Tanida, M., Sakatani, K., Takano, R., Tagai, K., 2004. Relation between asymmetry of prefrontal cortex activities and the autonomic nervous system during a mental arithmetic task: near infrared spectroscopy study. Neurosci. Lett. 369, 69–74.
Tian, F., Niu, H., Khan, B., Alexandrakis, G., Behbehani, K., Liu, H., 2011. Enhanced functional brain imaging by using adaptive filtering and a depth compensation algorithm in diffuse optical tomography. IEEE Trans. Med. Imaging 30 (6), 1239–1251.
Tong, Y., Frederick, B.D., 2010. Time lag dependent multimodal processing of concurrent fMRI and near-infrared spectroscopy (NIRS) data suggests a global circulatory origin for low-frequency oscillation signals in human brain. Neuroimage 53, 553–564.
Toronov, V., Franceschini, M., Filiaci, M., Fantini, S., Wolf, M., Michalos, A., Gratton, E., 2000. Near-infrared study of fluctuations in cerebral hemodynamics during rest and motor stimulation: temporal analysis and spatial mapping. Med. Phys. 27 (4), 801–815.
Toronov, V., Webb, A., Choi, J.H., Wolf, M., Michalos, A., Gratton, E., Hueber, D., 2001. Investigation of human brain hemodynamics by simultaneous near-infrared spectroscopy and functional magnetic resonance imaging. Med. Phys. 28, 521.
Toronov, V., Walker, S., Gupta, R., Choi, J.H., Gratton, E., Hueber, D., Webb, A., 2003. The roles of changes in deoxyhemoglobin concentration and regional cerebral blood volume in the fMRI BOLD signal. NeuroImage 19, 1521–1531.
Toronov, V.Y., Zhang, X., Webb, A.G., 2007. A spatial and temporal comparison of hemodynamic signals measured using optical and functional magnetic resonance imaging during activation in the human primary visual cortex. Neuroimage 34, 1136–1148.
Uludag, K., Müller-Bierl, B., Ugurbil, K., 2009. An integrative model for neuronal activity-induced signal changes for gradient and spin echo functional imaging. Neuroimage 48, 150–165.
Umeyama, S., Yamada, T., 2009a. New method of estimating wavelength-dependent optical path length ratios for oxy- and deoxyhemoglobin measurement using near-infrared spectroscopy. J. Biomed. Opt. 14 (5), 054038.
Umeyama, S., Yamada, T., 2009b. Monte Carlo study of global interference cancellation by multidistance measurement of near-infrared spectroscopy. J. Biomed. Opt. 14 (6), 064025.
Villringer, A., Chance, B., 1997. Non-invasive optical spectroscopy and imaging of human brain function. Trends Neurosci. 20, 435–442.
Wang, L., Jacques, S.L., 1995. Monte Carlo modeling of light transport in tissues. In: Welch, A.J., Van Gemert, M.J.C. (Eds.), Optical–Thermal Response of Laser-irradiated Tissue. Plenum, New York.
Wang, L., Jacques, S.L., Zheng, L., 1995. MCML — Monte Carlo modeling of light transport in multi-layered tissues. Comput. Methods Programs Biomed. 47, 131–146 (PubMed: 7587160).
Weiss, J., Ericsson, A., Astrom, G., Szomolanyi, P., Hemmingsson, A., 2001. High-resolution spectroscopic imaging of the human skin. Magn. Reson. Imaging 19, 275–278.
Wise, R.G., Ide, K., Poulin, M.J., Tracey, I., 2004. Resting fluctuations in arterial carbon dioxide induce significant low frequency variations in BOLD signal. Neuroimage 21 (4), 1652–1664.
Yamada, T., Umeyama, S., Matsuda, K., 2009. Multidistance probe arrangement to eliminate artifacts in functional near-infrared spectroscopy. J. Biomed. Opt. 16 (4), 06434.
Zeff, B.W., White, B.R., Dehghani, H., Schlaggar, B.L., Culver, J.P., 2007. Retinotopic mapping of adult human visual cortex with high-density diffuse optical tomography. Proc. Natl. Acad. Sci. U.S.A. 104 (29), 12169–12174.
Zenker, W., Kubik, S., 1996. Brain cooling in humans—anatomical considerations. Anat. Embryol. 193.
Zhang, R., Zuckerman, J.H., Iwasaki, K., Wilson, T.E., Crandall, C.G., Levine, B.D., 2002. Autonomic neural control of dynamic cerebral autoregulation in humans. Circulation 106 (14), 1814–1820.
Zhang, Q., Brooks, D.H., Franceschini, M.A., Boas, D.A., 2005. Eigenvector-based spatial filtering for reduction of physiological interference in diffuse optical imaging. J. Biomed. Opt. 10 (1), 011014.
Zhang, Q., Brown, E., Strangman, G., 2007a. Adaptive filtering for global interference cancellation and real-time recovery of evoked brain activity: a Monte Carlo simulation study. J. Biomed. Opt. 12 (4), 044014 (Jul.–Aug).
Zhang, Q., Brown, E., Strangman, G., 2007b. Adaptive filtering to reduce global interference in evoked brain activity detection: a human subject case study. J. Biomed. Opt. 12 (6), 064009 (Nov.–Dec. 2007b).
Zhang, Q., Strangman, G., Ganis, G., 2009. Adaptive filtering to reduce global interference in non-invasive NIRS measures of brain activation: how well and when does it work? Neuroimage 45 (3), 788–794.